

Learning Generative Adversarial Representations under Fairness and Censoring Constraints

Jiachun Liao Chong Huang Peter Kairouz Lalitha Sankar

Abstract

We present Generative Adversarial rePresentations (GAP) as a data-driven framework for learning censored and/or fair representations. GAP leverages recent advancements in adversarial learning to allow a data holder to learn universal representations that decouple a set of sensitive attributes from the rest of the dataset. Under GAP, finding the optimal fair/censoring encoder is formulated as a constrained minimax game between a data encoder and an adversary. We show that for appropriately chosen adversarial loss functions, GAP provides censoring guarantees against strong information-theoretic adversaries and enforces demographic parity. We also evaluate the performance of GAP on multi-dimensional Gaussian mixture models and real datasets, and show how a designer can certify that representations learned under an adversary with a fixed architecture perform well against more complex adversaries.

Keywords: Data censoring, Fairness, Adversarial Learning, Generative Adversarial Networks, Minimax Games, Information Theory

1 Introduction

The use of deep learning algorithms for data analytics has recently seen unprecedented success for a variety of problems such as image classification, natural language processing, and prediction of consumer behavior, electricity use, political preferences, to name a few. The success of these algorithms hinges on the availability of large datasets, that often contain sensitive information, and thus, may facilitate learning models that inherit societal biases leading to unintended algorithmic discrimination on legally protected groups such as race or gender. This, in turn, has led to data-censoring and fairness concerns and a growing body of research focused on developing representations of the dataset with fairness and/or censoring guarantees. These techniques predominantly involve designing randomizing schemes, and in recent years, distinct approaches with provable *statistical censoring or fairness* guarantees have emerged.

In the context of privacy, preserving the utility of published datasets while simultaneously providing provable privacy guarantees is a well-known challenge. While context-free privacy solutions, such as differential privacy [Dwork et al., 2006b,a, Dwork, 2008, Dwork and Roth, 2014], provide strong worst-case privacy guarantees, they often lead to a significant reduction in utility. In contrast, context-aware privacy solutions, e.g., mutual information privacy [Rebollo-Monedero et al., 2010, Calmon and Fawaz, 2012, Sankar et al., 2013, Salamatian et al., 2015, Basciftci et al., 2016], achieve improved privacy-utility tradeoff, but assume that the data holder has access to dataset statistics.

In the context of fairness, machine learning models seek to maximize predictive accuracy. Fairness concerns arise when models learned from datasets that include patterns of societal bias and discrimination inherit such biases. Thus, there is a need for actively decorrelating sensitive and non-sensitive data. In the context of publishing datasets or meaningful representations that can be “universally” used for a variety of learning tasks, modifying the training data is the most appropriate

and is the focus of this work. Fairness can then be achieved by carefully designing objective functions which approximate a specific fairness definition while simultaneously ensuring maximal utility [Zemel et al., 2013, Calmon et al., 2017, Ghassami et al., 2018]. This, in turn, requires dataset statistics.

Adversarial learning approaches for context-aware censoring and fairness have been studied extensively [Edwards and Storkey, 2015, Abadi and Andersen, 2016, Raval et al., 2017, Huang et al., 2017, Tripathy et al., 2017, Beutel et al., 2017, Madras et al., 2018b, Zhang et al., 2018]. They allow the data curator to cleverly decorrelate the sensitive attributes from the rest of the dataset. These approaches overcome the lack of statistical knowledge by taking a *data-driven approach* that leverages recent advancements in generative adversarial networks (GANs) [Goodfellow et al., 2014, Mirza and Osindero, 2014]. However, most existing efforts focus on extensive empirical studies without theoretical verification and focus predominantly on providing guarantees for a specific classification task.

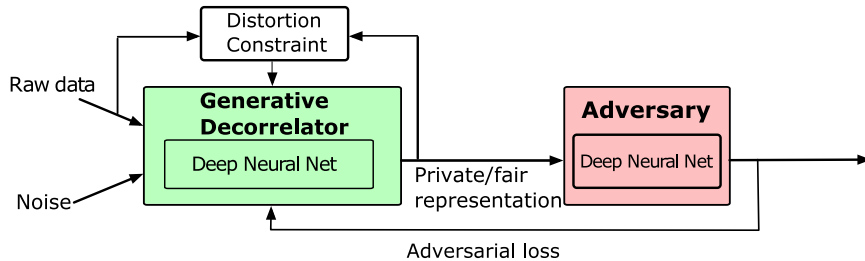


Figure 1: Generative adversarial model for privacy and fairness

1.1 Our Contributions.

This work introduces a general framework for context-aware censoring and fairness that we call *generative adversarial representation* (GAP) (see Figure 1). We provide precise connections to information-theoretic censoring and fairness formulations and derive game-theoretically optimal decorrelation schemes to compare against those learned directly from the data. While our framework can be generalized to learn an arbitrary representation using an encoder-decoder structure, this paper primarily focuses on learning censored/fair representations of the data (of the same dimension). We list our main contributions below.

When publishing a useful representation of the data for different learning tasks, it can be difficult to identify a set of target variables (labels) *a priori*. GAP allows us to publish representations that do not explicitly capture these downstream learning tasks. Instead, it ensures that the representation is close enough to the original data in some metric space thus ensuring good accuracy on downstream tasks for one or more non-sensitive labels.

1. We introduce GAP as a data-driven framework for creating fair and censored representations of data using an adversarially trained conditional generative model. Unlike existing works [Edwards and Storkey, 2016, Madras et al., 2018a, Chen et al., 2019], GAP can exploit different models (e.g., Figure 2) to create representations that are useful for a variety of classification and regression tasks, without requiring the designer to model these tasks at training time. We validate this observation via experiments on the GENKI [Whitehill and Movellan, 2012], HAR [Anguita et al., 2013], UCI, and UTK datasets using the two GAP architectures presented on the left of Figure 2.
2. We show that via the choice of the adversarial loss function, our framework can capture a rich class of statistical and information-theoretic adversaries. This allows us to compare data-driven approaches directly against strong inferential adversaries (e.g., a maximum *a posteriori*

probability (MAP) adversary with access to dataset statistics). We also show that by carefully designing the loss functions in the GAP framework, we can enforce demographic parity.

3. We make precise comparison between data-driven censoring/fairness methods and the minimax game-theoretic GAP formulation. For Gaussian mixture data, we derive game-theoretically optimal decorrelation schemes and compare them with those that are directly learned in a data-driven fashion to show that the gap between theory and practice is negligible. Furthermore, we propose using mutual information estimators to verify that no adversary (regardless of their computational power) can reliably infer the sensitive attribute from the learned representation.
4. We have provided a novel definition of censored representation and generalize the definition of demographic parity to representations, and therefore, generalize it to multiple/non-binary sensitive and label settings. By applying the GAP framework to datasets with non-binary sensitive features [Creager et al., 2019] (HAR,UCI Adult) and non-binary non-sensitive labels (UTK). We show the flexibility of GAP in hiding multiple sensitive features and preserving utilities of multiple applications. This is new in highlighting the generality of applying frequently used measures of fairness such as demographic parity to non-binary sensitive and label settings.

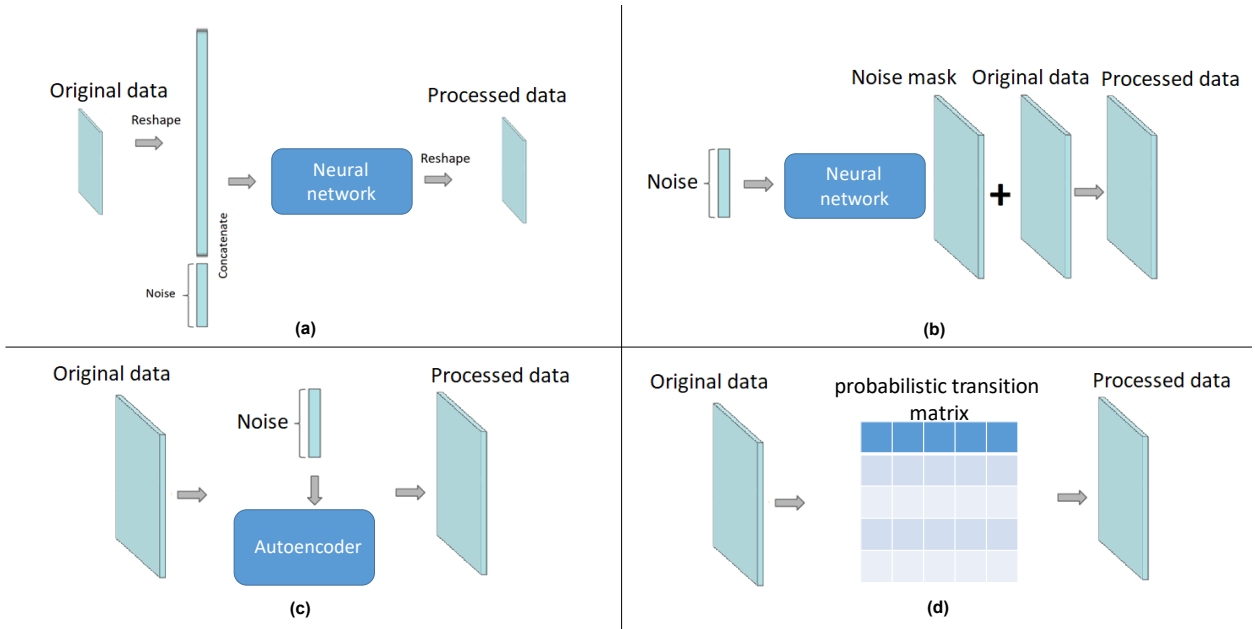


Figure 2: Different architectures of data processor (encoder) for GAP.

1.2 Related Work

In the context of publishing datasets with censoring and utility guarantees, a number of similar approaches have been recently considered. We briefly review them and clarify how our work is different. DP-based obfuscators for data publishing have been considered in [Hamm, 2016, Liu et al., 2017]. The author in [Hamm, 2016] considers a deterministic, compressive mapping of the input data with differentially private noise added either before or after the mapping. The approach in [Liu et al., 2017] relies on using deep auto-encoders to determine the relevant feature space to add differentially private noise, thereby eliminating the need to add noise to the original data. These novel approaches leverage minimax filters and deep auto-encoders to allow non-malicious entities to

learn some public features from the filtered data, while preventing malicious entities from learning other sensitive features. Both approaches incorporate a notion of context-aware privacy and achieve better privacy-utility tradeoffs while using DP to enforce privacy. However, DP can still incur a significant utility loss since it assumes worst-case dataset statistics. Our approach models a rich class of randomization-based schemes via a generative model that allows the generative decorrelator to tailor the noise to the dataset.

Our work is closely related to adversarial neural cryptography [Abadi and Andersen, 2016], learning censored representations [Edwards and Storkey, 2015], privacy preserving image sharing [Raval et al., 2017], privacy-preserving adversarial networks [Tripathy et al., 2017], and adversarially learning fair representation [Madras et al., 2018b] in which adversarial learning is used to learn how to protect communications by encryption or hide/remove sensitive information or generate fair representation of the data. Similar to these problems, our model includes a minimax formulation and uses adversarial neural networks to learn decorrelation schemes. However, in [Edwards and Storkey, 2015, Raval et al., 2017, Madras et al., 2018b], the authors use non-generative auto-encoders to remove sensitive information. Instead, we use a GANs-like approach to learn decorrelation schemes that prevent an adversary from inferring the sensitive variable. Furthermore, these formulations uses weighted combination of different loss functions to balance privacy with utility. We also go beyond in formulating a game-theoretic setting subject to a distortion constraint. These approaches are not equivalent because of the non-convexity (resp. concavity) of the minimax problem with respect to the decorrelator (resp. adversary) neural network parameters and requires new methods to enforce the distortion constraint during the training process. The distortion constraint allows us to directly limit the amount of distortion added to learn the private/fair representation for a variety of learning tasks, which is crucial for preserving the utility of the learned representation. Moreover, we compare the performance of the decorrelation schemes learned in an adversarial fashion with the game-theoretically optimal ones for canonical synthetic data models thereby providing formal verification of decorrelation schemes that are learned by competing against computational adversaries. Finally, we propose using mutual information as a criterion to certify that the representations we learned adversarially against an attacker with a fixed architecture generalize against unseen attackers with (possibly) more complex architecture.

Fair representations using information-theoretic objective functions and constrained optimization have been proposed in [Calmon et al., 2017, Ghassami et al., 2018]. However, both approaches require the knowledge of dataset statistics, which are very difficult to obtain for real datasets. We overcome the issue of statistical knowledge by taking a *data-driven approach*, i.e., learning the representation from the data directly via adversarial models. In contrast to in-processing approaches that modify learning algorithms to ensure fair predictions (e.g, using linear programs in [Dwork et al., 2012, Fish et al., 2016] or via adversarial learning approach in [Zhang et al., 2018]), we focus on a pre-processing approach to ensure fairness for a variety of learning tasks.

Generative adversarial networks (GANs) have recently received a lot of attention in the machine learning community [Goodfellow et al., 2014, Mirza and Osindero, 2014]. Ultimately, deep generative models hold the promise of discovering and efficiently internalizing the statistics of the target signal to be generated. Using GANs to generate synthetic non-sensitive attributes and labels which ensure fairness while preserving the utility of the data (predicting the label) has been studied in [Xu et al., 2018, Sattigeri et al., 2018]. The goal here is to develop a conditional GAN-based model to ensure fairness in the system by learning to generate a fairer synthetic dataset using an unconstrained minimax game with carefully designed loss functions corresponding with both fairness and utility. The synthetic data is generated by a conditional generative adversarial network (GAN) which generates the non-sensitive attributes-label pair given the noise variable and the sensitive attribute. The utility is preserved by generating data that is very similar to the original data. To ensure fairness, the generator generates data samples such that an auxiliary classifier trained to

predict the sensitive attribute from the synthetic data performs as poorly as possible. The methods presented in these papers are very different from our method since we are focusing on creating a fair/private representations of the original data while preserving the utility of the representation for a variety of learning tasks. There are different ways for enforcing fairness, and our work presents a framework that aids in achieving this goal. More work is needed to be done in this area.

1.3 Outline

The remainder of our paper is organized as follows. We formally defined censored and fair representations in Section 2. In Section 3, we formalize our GAP model and highlight the theoretical guarantees of this approach. In Section 4, we present theoretical results for datasets modeled as multi-dimensional Gaussian mixtures. Finally, we showcase the performance of GAP on the GENKI, HAR, UCI Adult, and UTKFace datasets in Section 5. All proofs and algorithms are deferred to appendices in the accompanying supplementary materials.

2 Preliminaries

We consider a dataset \mathcal{D} with n entries where each entry is denoted as (S, X, Y) where $S \in \mathcal{S}$ is a collection of sensitive features, $X \in \mathcal{X}$ is a collection of non-sensitive features, and $Y \in \mathcal{Y}$ is the collection of target (non-sensitive) features to be learned. Let $\hat{Y} \in \mathcal{Y}$ be a prediction of Y . We note that S , X , and Y can be a collection of features or labels (e.g., S can be gender, race, and sexual orientation, while Y could be age, facial expression, etc.); for ease of writing, we use the term variable to denote both single and multiple features/labels.

Instances of X , S , and Y are denoted by x , s and y , respectively. We assume that each entry (X, S, Y) is independent and identically distributed (i.i.d.) according to $P(X, S, Y)$.

Recent results on fairness in learning applications guarantees that for a specific target variable, the prediction of a machine learning model is accurate with respect to (*w.r.t.*) the target variable but unbiased *w.r.t.* a sensitive variable. The three oft-used fairness measures are demographic parity, equalized odds, and equality of opportunity. Demographic parity imposes the strongest fairness requirement via complete independence of the prediction of the target variable and sensitive variable, and thus, least favors (for correlated target and sensitive variables) utility [Hardt et al., 2016]. Equalized odds ensures this independence conditioned on the target variable thereby ensuring equal rates for true and false positives (wherein the target variable is binary) for all demographics. Equal opportunity ensures equalized odds for the true positive case alone [Hardt et al., 2016].

For the sake of completeness, we review these definitions briefly. We note that these definitions are often aimed at sensitive (S) and target (Y) features that are binary, and in reviewing these definitions below, we make this assumption too. However, we note that these definitions can be generalized to the non-binary setting; indeed, our own generalizations of these definitions as applied to representation setting do not make such an assumption.

Definition 1 ([Hardt et al., 2016]) A predictor $f(S, X) = \hat{Y}$ satisfies

- demographic parity *w.r.t.* the sensitive variable S , if \hat{Y} and S are independent, i.e.,

$$\Pr(\hat{Y} = 1|S = 1) = \Pr(\hat{Y} = 1|S = 0) \quad (1)$$

- equalized odds *w.r.t.* the sensitive variable S and target variable Y , if \hat{Y} and S are independent conditional on Y , i.e.,

$$\Pr(\hat{Y} = 1|S = 1, Y = y) = \Pr(\hat{Y} = 1|S = 0, Y = y), \quad y \in \{0, 1\} \quad (2)$$

- equality of opportunity w.r.t. the sensitive variable S and target variable Y , if \hat{Y} and S are independent conditional on $Y = 1$, i.e.,

$$\Pr(\hat{Y} = 1|S = 1, Y = 1) = \Pr(\hat{Y} = 1|S = 0, Y = 1). \quad (3)$$

We begin by first defining the notions of censoring and fairness for representations. In particular, as discussed thus far, in the censoring context, our goal is to introduce a definition that ensures that the censored representation limits leakage of sensitive variables from adversaries that can potentially *learn* it from the released data. It is crucial to note that censoring will in general not give the kind of strong privacy guarantees provided by differential privacy but can be relevant for some applications where releasing a representation is crucial.

Definition 2 (Censored Representations) *A representation X_r of X is censored w.r.t. the sensitive variable S against a learning adversary $h(\cdot)$, whose performance is evaluated via a loss function $\ell(h(X_r), S)$, if for an optimal adversarial strategy $h_g^* = \operatorname{argmin}_h \mathbb{E}[\ell(h(g(X)), S)]$ corresponding to any (randomized) function $g(X)$*

$$\mathbb{E}[\ell(h_g^*(g(X)), S)] \leq \mathbb{E}[\ell(h_g^*(X_r), S)], \quad (4)$$

where $X_r = g^*(X)$ and the expectation is over h , g , X , and S .

To motivate the generation of fair representations, we now extend the definition of demographic parity for representations. Indeed it is known that fair representations can be used to ensure fair classification (see, for example, [Hardt et al., 2016]). We formally define fair representation and prove that such representations ensure fair classification.

Definition 3 (Fair Representations) *Let \mathcal{X}_r and \mathcal{S} be the supports of X_r and S , respectively. A representation X_r of X satisfies demographic parity w.r.t. the sensitive variable S if X_r and S are independent, i.e., for any $x_r \in \mathcal{X}_r$ and $s, s' \in \mathcal{S}$,*

$$\Pr(X_r = x_r|S = s) = \Pr(X_r = x_r|S = s'). \quad (5)$$

Given this definition, we now prove that a fair representation in the sense of demographic parity will guarantee that any downstream learning algorithm making use of the fair representation is fair (in the sense of demographic parity) w.r.t. the sensitive label S .

Theorem 1 (Fair Learning via Fair Representation) *Given a dataset consisting of sensitive, non-sensitive, and target variables (S, X, Y) , respectively, if a fair representation $X_r = g(X)$ satisfies demographic parity w.r.t. S , then any learning algorithm $f : \mathcal{X}_r \rightarrow \mathcal{Y}$ satisfies demographic parity w.r.t. S .*

The proof of Theorem 1 is in Appendix A.

Remark 1 *Note that the definitions of equalized odds and equality of opportunity in Def. 1 explicitly involve a downstream learning application, and therefore, the design of a fair representation needs to include a classifier explicitly. In contrast to the universal representation setting considered here, such targeted representations and the ensuing fair classifiers provide guarantees only for those targeted Y features. In this limited context, however, one can still define a representation X_r as ensuring equalized odds (w.r.t. to S) in classifying Y if the predicted output learned from X_r , i.e., $\hat{Y}(X_r)$, is independent of S conditioned on Y .*

One simple approach to obtain a fair/censored representation X_r is by choosing $X_r = N$ where N is a random variable independent of X and S . However, such an X_r has no downstream utility (quantified, for example, via downstream task accuracy). More generally, the design of X_r has to ensure utility, and thus, there is a tradeoff between guaranteeing fairness/censoring and assuring a desired level of utility. GAP enables quantifying these tradeoffs formally as described in the next section.

3 Generative Adversarial Representations

Formally, GAP involves two components, an encoder and an adversary as shown in Fig. 1. The goal of the encoder $g : \mathcal{X} \times \mathcal{S} \rightarrow \mathcal{X}_r$ is to actively decorrelate S from X while that of the adversary $h : \mathcal{X}_r \rightarrow \mathcal{S}$ is to infer S . Thus, in general, $g(X, S)$ is a randomized mapping that outputs a representation $X_r = g(X, S)$. Note that the design of $g(\cdot)$ depends on both X and S ; however, we note that S *may not necessarily* be an input to the encoder though it will always affect the design of $g(\cdot)$ via the adversarial training process. In contrast, the role of the adversary is captured via $h(X_r)$, the adversarial decision rule (classifier) in inferring the sensitive variable S as $\hat{S} = h(g(X))$ from the representation $g(X, S)$. In general, the hypothesis h can be a *hard decision rule* under which $h(g(X))$ is a direct estimate of S or a *soft decision rule* under which $h(g(X)) = P_h(\cdot|g(X))$ is a distribution over \mathcal{S} .

To quantify the adversary’s performance, we use a loss function $\ell(h(g(X = x)), S = s)$ defined for every pair (x, s) . Thus, the adversary’s expected loss *w.r.t.* X and S is $L(h, g) \triangleq \mathbb{E}[\ell(h(g(X)), S)]$, where the expectation is taken over $P(X, S)$ and the randomness in g and h .

Intuitively, the generative (since it randomizes to decorrelate) encoder would like to minimize the adversary’s ability to learn S reliably from X_r . This can be trivially achieved by releasing an X_r independent of X . However, such an approach provides no utility for data analysts who want to learn non-sensitive variables Y from X_r . To overcome this issue, we capture the loss incurred by perturbing the original data via a distortion function $d(x_r, x)$, which measures how far the original data $X = x$ is from the processed data $X_r = x_r$. Ensuring statistical utility in turn requires constraining the average distortion $\mathbb{E}[d(g(X), X)]$ where the expectation is taken over $P(X, S)$ and the randomness in g .

3.1 GAP: Framework and Theoretical Results

To publish a censored or fair representation X_r , the data curator wishes to learn an encoder g that guarantees both censoring/fairness (in the sense that it is difficult for the adversary to learn S from X_r) as well as utility (in the sense that it does not distort the original data too much). In contrast, for a fixed encoder g , the adversary would like to find a (potentially randomized) function h that minimizes its expected loss, which is equivalent to maximizing the negative of the expected loss. This leads to a constrained minimax game between the encoder and the adversary given by

$$\min_{g(\cdot)} \max_{h(\cdot)} - \mathbb{E}[\ell(h(g(X)); S)], \tag{6a}$$

$$s.t. \quad \mathbb{E}[d(g(X), X)] \leq D. \tag{6b}$$

where the constant $D \geq 0$ determines the allowable distortion of the representation and the expectation is taken over $P(X, S)$ and the randomness in g and h .

Theorem 2 *For sufficiently large distortion bound D , the constrained minimax optimization in (6) generates a GAP X_r that is censored w.r.t. to S .*

	Loss function $\ell(h(g(X)), s)$	Optimal adversarial strategy h^*	Adversary type
Squared loss	$(h(g(X)) - S)^2$	$\mathbb{E}[S g(X)]$	MMSE adversary
0-1 loss	$\begin{cases} 0 & \text{if } h(g(X)) = S \\ 1 & \text{otherwise} \end{cases}$	$\operatorname{argmax}_{s \in \mathcal{S}} P(s g(X))$	MAP adversary
Log-loss	$\log \frac{1}{P_h(s g(X))}$	$P(s g(X))$	Belief refining adversary
α -loss	$\frac{\alpha}{\alpha-1} \left(1 - P_h(s g(X))^{1-\frac{1}{\alpha}}\right)$	$\frac{P(s g(X))^\alpha}{\sum_{s \in \mathcal{S}} P(s g(X))^\alpha}$	Generalized belief refining adversary

Table 1: GAP under various loss functions

Our GAP framework places no restrictions on the adversary. Indeed, different loss functions and decision rules lead to different adversarial models (see Table 1). The versatility of GAP to a large class of (inferring) adversarial models is captured by using the recently introduced tunable α -loss function $\ell(h(g(X)), s) = \frac{\alpha}{\alpha-1} \left(1 - P_h(s|g(X))^{1-\frac{1}{\alpha}}\right)$, $\alpha \in [1, \infty]$ [Liao et al., 2018]. The authors in [Liao et al., 2018] show that by tuning the parameter $\alpha \in [1, \infty]$, α -loss captures a variety of information-theoretic adversaries ranging from a hard-decision adversary (for $\alpha = 1$) via the 0-1 loss function $\ell(h(g(X)), s) = \mathbb{I}_{h(g(X)) \neq s}$ ¹ to a soft-decision adversary (for $\alpha = \infty$) under the log-loss function $\ell(h(g(X)), s) = -\log P_h(s|g(X))$. Thus, for a given $g(\cdot)$, under α -loss, the optimal adversarial strategy is given by the following proposition (also in the last row of Table 1).

Proposition 1 *Under α -loss, the optimal adversary decision rule is a ‘ α -tilted’ conditional distribution $P_h^*(s|g(X)) = \frac{P(s|g(X))^\alpha}{\sum_{s \in \mathcal{S}} P(s|g(X))^\alpha}$. The optimization in (6) reduces to $\min_{g(\cdot)} -H_\alpha^A(S|g(X))$, where $H_\alpha^A(\cdot|\cdot)$ is the Arimoto conditional entropy.*

Note that for $\alpha = 1$ and $\alpha = \infty$, the optimal adversarial strategies reduce to those for log-loss (third row) and 0-1 loss (second row), respectively.

Corollary 1 *Using α -loss, we can obtain a continuous interpolation between a hard-decision adversary under 0-1 loss ($\alpha \rightarrow \infty$) and a soft-decision adversary under log-loss function ($\alpha \rightarrow 1$).*

Note that under the hard-decision rules in which the adversary uses a 0-1 loss function, the optimal adversarial strategy is the maximum a posteriori (MAP) decision rule and the GAP minimax problem in (6) simplifies to $\min_{g(\cdot)} \max_{s \in \mathcal{S}} P(s, g(X)) - 1$. For a soft-decision adversary under log-loss, the optimal adversarial strategy h^* is $P(S|g(X))$ and the GAP minimax problem in (6) simplifies to $\min_{g(\cdot)} -H(S|g(X)) = \min_{g(\cdot)} I(g(X), S)$ for known prior of S subject to $\mathbb{E}[d(g(X), X)] \leq D$, where $I(g(X), S)$ is the mutual information (MI) between $g(X)$ and S . Based on this observation, we have the following theorem.

Theorem 3 *Under α -loss (including log-loss and 0-1 loss), GAP enforces fairness subject to the distortion constraint. As the distortion increases, the ensuing fairness guarantee approaches ideal demographic parity.*

The proofs of Theorem 2, Proposition 1, Corollary 1 and Theorem 3 are presented in Appendix B. Many notions of fairness rely on computing probabilities to ensure independence of sensitive and

¹Note that for $\alpha = \infty$, α -loss reduces to probability of error, for which the optimal adversarial strategy that minimizes the expected loss is the *maximal a posteriori* (MAP) rule and the resulting probability of error is the 0-1 loss.

target variables that are not easy to optimize in a data-driven fashion. In Theorem 3, we propose α -loss (including log-loss modeled in practice via cross-entropy) in GAP as a proxy for enforcing fairness.

A predominant approach in the literature in the context of representations and fairness is to explicitly include the intended classification task, i.e., design representations for a specific learning task. Our GAP formulation can be extended to include this special case. As one may expect, this requires including an additional constraint to ensure high accuracy in learning Y thereby allowing us to specialize (6) to obtain the following minimax game:

$$\min_{g'(\cdot), f(\cdot)} \max_{h(\cdot)} -\mathbb{E}[\ell(h(g'(X))); S] + \lambda \mathbb{E}[\ell'(f(g'(X)), Y)], \quad (7a)$$

$$s.t. \quad \mathbb{E}[d(g'(X), X)] \leq D, \quad (7b)$$

where $f(\cdot)$ be a classifier for a target feature Y , $\lambda > 0$, and $g'(\cdot)$ and $h(\cdot)$ are the encoder and the adversarial classifier, respectively, as in (6). Note that the loss functions $\ell(\cdot)$ and $\ell'(\cdot)$ can be different. The transformation in (7) is more complicate than the GAP framework but produces a fair classifier for the target feature and a fair representation, denoted by X'_r , for any other downstream applications, simultaneously. We will evaluate the effect of incorporating a downstream application by comparing the utility of the $f(\cdot)$ in (7) and a classifier generated by using $X_r = g(\cdot)$ in (6) for the target feature.

In the GAP framework, we generate fair representations to guarantee fairness (in term of demographic parity) in downstream applications for any subset of target features. Another common method to provide fairness guarantee is to generate a fair predictor/classifier for the target variable. We show the transformation of the GAP framework which designs a fair predictor/classifier as follow.

Let $\hat{Y} = \tilde{g}(S, X)$ be a predictor/classifier for the targeted variable Y . Note that the $\tilde{g}(\cdot)$ generally depends on both X and S but the dependence on S can be implicit for scenarios where the sensitive information S is not allowed to be used. Let h be a decision rule used by the adversary to infer the sensitive variable S as $\hat{S} = h(\tilde{g}(S, X), Y)$ from the true targeted variable Y and the soft information of the predictor $\tilde{g}(S, X) = P_{\hat{Y}|X,S}$. Analogy to (6), the design of a fair predictor/classifier can be formulated as

$$\min_{\tilde{g}(\cdot)} \max_{h(\cdot)} -\mathbb{E}[\ell(h(\tilde{g}(S, X), Y), S)], \quad (8a)$$

$$s.t. \quad \mathbb{E}[\ell(\tilde{g}(S, X), Y)] \leq L. \quad (8b)$$

Proposition 2 *Under α -loss (incorporating both log-loss and 0-1 loss), the GAP formulation in (8) enforces fairness subject to the expected loss constraint. As the loss increases, the ensuing fairness guarantee approaches ideal equalized odd of \tilde{g} respect to the sensitive variable S and the targeted variable Y .*

The proof of Proposition 2 is in Appendix B.5. Note that the formulation in (8) can also be used to generate a fair predictor or classifier in term of demographic parity or equality of opportunity. Specifically, for demographic parity, the adversary will only have $\tilde{g}(S, X)$ as the input and for equality of opportunity, the adversary will have both $\tilde{g}(S, X)$ and $Y = 1$ as the input.

3.2 Data-driven GAP

Thus far, we have focused on a setting where the data holder has access to $P(X, S)$. When $P(X, S)$ is known, the data holder can simply solve the constrained minimax optimization problem in (6) (game-theoretic version of GAP) to obtain a decorrelation scheme that would perform best against a

chosen type of adversary. In the absence of $P(X, S)$, we propose a data-driven version of GAP that allows the data holder to learn decorrelation schemes directly from a dataset $\mathcal{D} = \{(x_{(i)}, s_{(i)})\}_{i=1}^n$. Under the data-driven version of GAP, we represent the decorrelation scheme via a generative model $g(X; \theta_p)$ parameterized by θ_p . This generative model takes X as input and outputs X_r . In the training phase, the data holder learns the optimal parameters θ_p by competing against a *computational adversary*: a classifier modeled by a neural network $h(g(X; \theta_p); \theta_a)$ parameterized by θ_a . In the evaluation phase, the performance of the learned decorrelation scheme can be tested under a strong adversary that is computationally unbounded and has access to dataset statistics. We follow this procedure in the next section.

In theory, the functions h and g can be arbitrary. However, in practice, we need to restrict them to a rich hypothesis class. Figure 1 shows an example of the GAP model in which the generative decorrelator and adversary are modeled as deep neural networks. For a fixed h and g , if S is binary, we can quantify the adversary’s *empirical loss* using cross entropy $L_n(\theta_p, \theta_a) = -\frac{1}{n} \sum_{i=1}^n s_{(i)} \log h(g(x_{(i)}; \theta_p); \theta_a) + (1 - s_{(i)}) \log(1 - h(g(x_{(i)}; \theta_p); \theta_a))$. It is easy to generalize cross entropy to the multi-class case using the softmax function. The optimal model parameters are the solutions to

$$\min_{\theta_p} \max_{\theta_a} -L_n(\theta_p, \theta_a), \quad s.t. \quad \mathbb{E}_{\mathcal{D}}[d(g(X; \theta_p), X)] \leq D, \quad (9)$$

where the expectation is over \mathcal{D} and the randomness in g .

The minimax optimization in (9) is a two-player non-cooperative game between the generative decorrelator and the adversary with strategies θ_p and θ_a , respectively. In practice, we can learn the equilibrium of the game using an iterative algorithm (see Algorithm 1 in Appendix C). We first maximize the negative of the adversary’s loss function in the inner loop to compute the parameters of h for a fixed g . Then, we minimize the decorrelator’s loss function, which is modeled as the negative of the adversary’s loss function, to compute the parameters of g for a fixed h . Observe that the distortion constraint in (9) makes our minimax problem different from what is extensively studied in previous works. To incorporate the distortion constraint, we use the *penalty method* [Lillo et al., 1993] to replace the constrained optimization problem by adding a penalty to the objective function. The penalty consists of a penalty parameter ρ_t multiplied by a measure of violation of the constraint at the t^{th} iteration. The constrained optimization problem of the generative decorrelator can be approximated by a series of unconstrained optimization problems with the loss function $L_n(\theta_p, \theta_a) + \rho_t(\max\{0, \mathbb{E}[d(g(x_{(i)}; \theta_p), x_{(i)})] - D\})^2$, where ρ_t is a penalty coefficient increases with the number of iterations t . The algorithm and the penalty method are detailed in Appendix C.

4 GAP for Gaussian Mixture Models

In this section, we focus on a setting where $S \in \{0, 1\}$ and X is an m -dimensional Gaussian mixture random vector whose mean is dependent on S . Let $P(S = 1) = q$. Let $X|S = 0 \sim \mathcal{N}(-\mu, \Sigma)$ and $X|S = 1 \sim \mathcal{N}(\mu, \Sigma)$, where $\mu = (\mu_1, \dots, \mu_m)$, and without loss of generality, we assume that $X|S = 0$ and $X|S = 1$ have the same covariance Σ .

We consider a MAP adversary who has access to $P(X, S)$ and the privacy mechanism. The encoder’s goal is to sanitize X in a way that minimizes the adversary’s probability of correctly inferring S from X_r . In order to have a tractable model for the encoder, we mainly focus on linear (precisely affine) GAP $X_r = g(X) = X + Z + \beta$, where Z is an independently generated noise vector. This linear GAP enables controlling both the mean and covariance of the privatized data. To quantify utility of the privatized data, we use the ℓ_2 distance between X and X_r as a distortion measure to obtain a distortion constraint $\mathbb{E}_{X, X_r} \|X - X_r\|^2 \leq D$.

4.1 Game-Theoretical Approach

Consider the setup where both the encoder and the adversary have access to $P(X, S)$. Further, let Z be a zero-mean multi-dimensional Gaussian random vector. Although other distributions can be considered, we choose additive Gaussian noise for tractability reasons.

Without loss of generality, we assume that $\beta = (\beta_1, \dots, \beta_m)$ is a constant parameter vector and $Z \sim \mathcal{N}(0, \Sigma_p)$. Following similar analysis in Gallager [2013], we can show that the adversary's probability of detection is given by

$$P_d^{(G)} = qQ\left(-\frac{\alpha}{2} + \frac{1}{\alpha} \ln\left(\frac{1-q}{q}\right)\right) + (1-q)Q\left(-\frac{\alpha}{2} - \frac{1}{\alpha} \ln\left(\frac{1-q}{q}\right)\right), \quad (10)$$

where $\alpha = \sqrt{(2\mu)^T(\Sigma + \Sigma_p)^{-1}2\mu}$. Furthermore, since $\mathbb{E}_{X, X_r}[d(X_r, X)] = \mathbb{E}_{X, X_r}\|X - X_r\|^2 = \mathbb{E}\|Z + \beta\|^2 = \|\beta\|^2 + \text{tr}(\Sigma_p)$, the distortion constraint implies that $\|\beta\|^2 + \text{tr}(\Sigma_p) \leq D$. To make the problem more tractable, we assume both X and Z are independent multi-dimensional Gaussian random vectors with diagonal covariance matrices.

Theorem 4 Consider GAP given by $g(X) = X + Z + \beta$, where $X|S$ and Z are multi-dimensional Gaussian random vectors with diagonal covariance matrices Σ and Σ_p . Let $\{\sigma_1^2, \dots, \sigma_m^2\}$ and $\{\sigma_{p_1}^2, \dots, \sigma_{p_m}^2\}$ be the diagonal entries of Σ and Σ_p , respectively. The parameters of the minimax optimal privacy mechanism are

$$\beta_i^* = 0, \quad \sigma_{p_i}^{*2} = \left(\frac{|\mu_i|}{\sqrt{\lambda_0^*}} - \sigma_i^2, 0\right)^+, \quad \forall i = \{1, 2, \dots, m\},$$

where λ_0^* is chosen such that $\sum_{i=1}^m \left(\frac{|\mu_i|}{\sqrt{\lambda_0^*}} - \sigma_i^2\right)^+ = D$. For this optimal mechanism, the accuracy of the MAP adversary is given by (10) with $\alpha = 2 \sqrt{\frac{\sum_{i=1}^m \mu_i^2}{\sigma_i^2 + \left(\frac{|\mu_i|}{\sqrt{\lambda_0^*}} - \sigma_i^2\right)^+}}$.

The proof of Theorem 4 is provided in Appendix C.1. We observe that when σ_i^2 is greater than some threshold $\frac{|\mu_i|}{\sqrt{\lambda_0^*}}$, no noise is added to the data on this dimension due to the high variance.

When σ_i^2 is smaller than $\frac{|\mu_i|}{\sqrt{\lambda_0^*}}$, the amount of noise added to this dimension is proportional to $|\mu_i|$; this is intuitive since a large $|\mu_i|$ indicates the two conditionally Gaussian distributions are further away on this dimension, and thus, distinguishable. Thus, more noise needs to be added in order to reduce the MAP adversary's inference accuracy.

4.2 Data-driven Approach

For the data-driven linear GAP, we assume the encoder only has access to the dataset \mathcal{D} with n data samples but not the actual distribution of (X, S) . Computing the optimal privacy mechanism becomes a learning problem. In the training phase, the data holder learns the parameters of the GAP by competing against a computational adversary modeled by a multi-layer neural network. When convergence is reached, we evaluate the performance of the learned mechanism by comparing with the one obtained from the game-theoretic approach. To quantify the performance of the learned GAP, we compute the accuracy of inferring S under a strong MAP adversary that has access to both the joint distribution of (X, S) and the privacy mechanism.

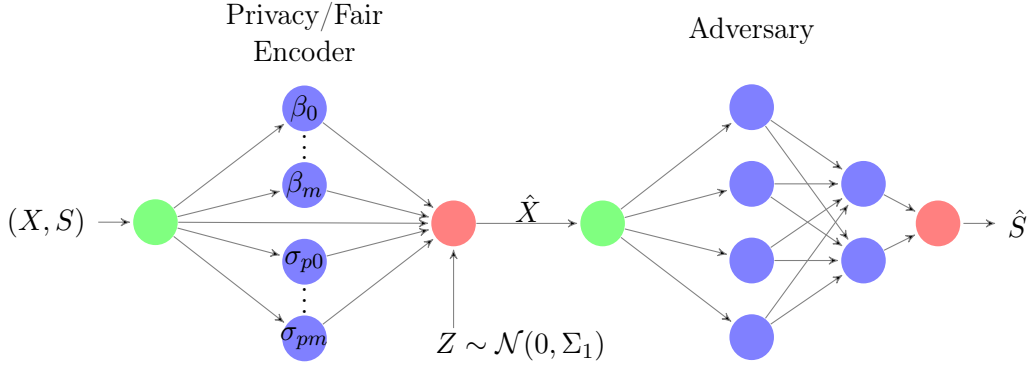


Figure 3: Neural network structure of linear GAP for Gaussian mixture data

Since the sensitive variable S is binary, we measure the training loss of the adversary network by the empirical log-loss function

$$L_n(\theta_p, \theta_a) = -\frac{1}{n} \sum_{i=1}^n s_{(i)} \log h(g(x_{(i)}; \theta_p); \theta_a) + (1 - s_{(i)}) \log(1 - h(g(x_{(i)}; \theta_p); \theta_a)). \quad (11)$$

For a fixed encoder parameter θ_p , the adversary learns the optimal θ_a^* by maximizing (11). For a fixed θ_a , the encoder learns the optimal θ_p^* by minimizing $-L_n(h(g(X; \theta_p); \theta_a), S)$ subject to the distortion constraint $\mathbb{E}_{X, X_r} \|X - X_r\|^2 \leq D$.

As shown in Figure 3, the encoder is modeled by a two-layer neural network with parameters $\theta_p = \{\beta_0, \dots, \beta_m, \sigma_{p0}, \dots, \sigma_{pm}\}$, where β_k and σ_{pk} represent the mean and standard deviation for each dimension $k \in \{1, \dots, m\}$, respectively. The random noise Z is drawn from a m -dimensional independent zero-mean standard Gaussian distribution with covariance Σ_1 . Thus, we have $\hat{X}_k = X_k + \beta_k + \sigma_{pk} Z_k$. The adversary, whose goal is to infer S from privatized data X_r , is modeled by a three-layer neural network classifier with leaky ReLU activations.

To incorporate the distortion constraint into the learning process, we add a penalty term to the objective of the encoder. Thus, the training loss function of the encoder is given by

$$L(\theta_p, \theta_a) = L_n(\theta_p, \theta_a) + \rho \max\{0, \frac{1}{n} \sum_{i=1}^n d(g(x_{(i)}; \theta_p), x_{(i)}) - D\}, \quad (12)$$

where ρ is a penalty coefficient which increases with the number of iterations. The added penalty consists of a penalty parameter ρ multiplied by a measure of violation of the constraint. This measure of violation is non-zero when the constraint is violated. Otherwise, it is zero.

4.3 Illustration of Results

We use synthetic datasets to evaluate the performance of the learned GAP. Each dataset contains $20K$ training samples and $2K$ test samples. Each data entry is sampled from an independent multi-dimensional Gaussian mixture model. We consider two categories of synthetic datasets with $P(S = 1)$ equal to 0.75 and 0.5, respectively. Both the encoder and the adversary in the GAP framework are trained on Tensorflow Abadi et al. [2016] using Adam optimizer with a learning rate of 0.005 and a minibatch size of 1000. The distortion constraint is enforced by the penalty method as detailed in supplement B (see (35)).

Figure 4 illustrates the performance of the learned GAP scheme against a strong theoretical MAP adversary for a 32-dimensional Gaussian mixture model with $P(S = 1) = 0.75$ and 0.5. We

observe that the inference accuracy of the MAP adversary decreases as the distortion increases and asymptotically approaches (as expected) the prior on the sensitive variable. The decorrelation scheme obtained via the data-driven approach performs very well when pitted against the MAP adversary (maximum accuracy difference around 0.7% compared to the theoretical optimal). Furthermore, the estimated mutual information decreases as the distortion increases. In other words, for the data generated by Gaussian mixture model with binary sensitive variable, the data-driven version of GAP can learn decorrelation schemes that perform as well as the decorrelation schemes computed under the theoretical version of GAP, given that the generative decorrelator has access to the statistics of the dataset.

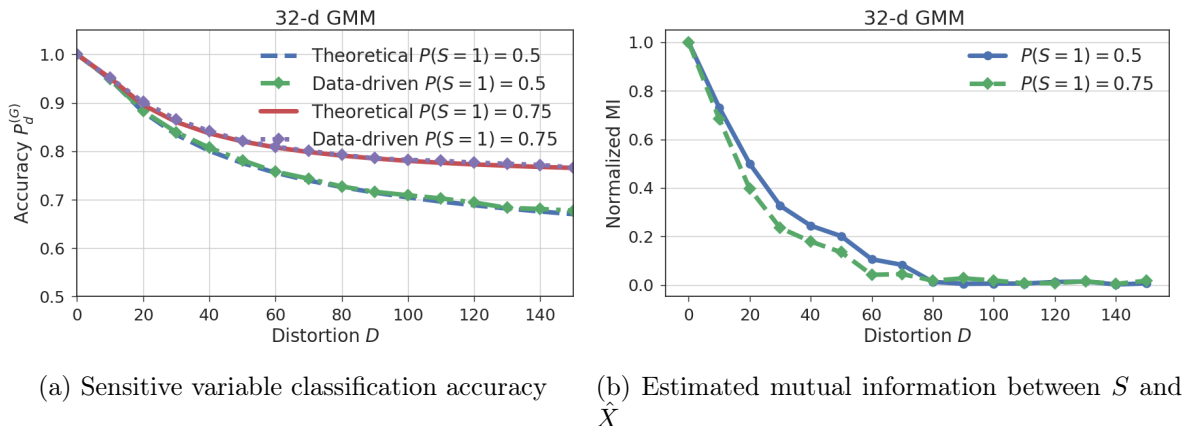


Figure 4: Performance of GAP for Gaussian mixture models

5 GAP for Real Datasets

We apply our GAP framework to real-world datasets to demonstrate its effectiveness in various aspects:

- GENKI and HAR datasets are used to show the advantage of GAP in providing censoring guarantee against a belief-refining adversary (captured by log-loss) who is interested in a sensitive feature, e.g., gender or identities of individuals, and also to show the effectiveness of the GAP framework on estimating mutual information.
- UCI Adult dataset² is used to show the effectiveness of the GAP framework in approaching demographic parity for both binary and non-binary sensitive features.
- UTKFace dataset³ is used to demonstrate the effectiveness of the GAP framework in multiple downstream applications: including a non-binary classification of ethnicity and ordinal regression of age.

In the experiments, we consider the first three different decorrelator architectures in Figure 2: the feedforward neural network decorrelator (FNND), the transposed convolution neural network decorrelator (TCNND) and the noisy autoencoder decorrelator (NoisyAED). The FNND architecture (shown in Figure 2 (a)) uses a feedforward multi-layer neural network to combine the low-dimensional random noise and the original data (i.e., X or (S, X)) together. The TCNND (shown

²<https://archive.ics.uci.edu/ml/datasets/adult>

³<http://aicp.eecs.utk.edu/wiki/UTKFace>

in Figure 2 (b)) takes a low-dimensional random noise and generates high-dimensional noise using a multi-layer transposed convolution neural network. The generated high-dimensional noise is added to the original data to produce the processed data (i.e., the representation X_r). The NoisyAED (shown in Figure 2 (c)) uses the encoding part of an autoencoder to generate a lower-dimensional feature vector of the original data and adds independent random noise to each element of the feature vector. The decoding part of the autoencoder reconvert the noise-adding feature vector to an representation of the original data, i.e., the the processed data X_r . We apply both the FNND and TCNND architectures to the GENKI dataset. For the UCI Adult and HAR datasets, we use the FNND architecture, and the NoisyAED architecture is applied to the UTKFace dataset.

We use the accuracy of predicting a sensitive feature as the measure of censoring. For fairness, given an arbitrary prediction $\hat{Y} = y$, demographic parity requires **zero** differences between the conditional probabilities of $\hat{Y} = y$ given different realizations of the sensitive feature S . We take the maximal difference as the measure of demographic parity fairness, i.e.,

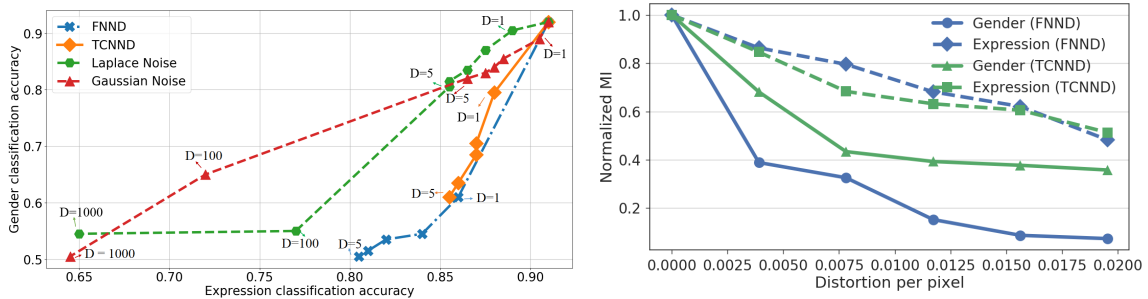
$$\Delta_{\text{DemP}}(y) = \max_{s, s' \in \mathcal{S}} |P(\hat{Y} = y | S = s) - P(\hat{Y} = y | S = s')| \quad (13)$$

and a smaller value of Δ_{DemP} implies a better approximation of the demographic parity fairness. We illustrate the results for each dataset mentioned above in the following subsections. Details of all experiments on these datasets are in Appendix F.

5.1 Illustration of Results for GENKI Dataset

Figure 5a illustrates the gender classification accuracy of the adversary for different values of distortion. It can be seen that the adversary’s accuracy of classifying the sensitive variable (gender) decreases progressively as the distortion increases. Given the same distortion value, FNND achieves lower gender classification accuracy compared to TCNND. An intuitive explanation is that the FNND uses both the noise vector and the original image to generate the processed image. However, the TCNND generates the noise mask that is independent of the original image pixels and adds the noise mask to the original image in the final step.

Differential privacy has emerged as the gold standard for data privacy. In this experiment, we vary the variance of the Laplace and Gaussian noise to connect the noise adding mechanisms to local differential privacy [Duchi et al., 2013, Kairouz et al., 2016]. In particular, we compute the differential privacy guarantees provided by independent Laplace and Gaussian noise adding mechanisms for different distortion values. The details are provided in Appendix E. In Table 2, we observe that even if a huge amount of noise is added to each pixel of the image, the privacy risk (ϵ) is still high. Furthermore, adding a huge noise deteriorates the expression classification accuracy.



(a) Gender vs. expression classification accuracy (b) Normalized mutual information estimation

Figure 5: CUT and mutual information estimation for GENKI

Distortion D	1	2	3	4	5	100	1000
Laplace Mechanism ϵ	5792.61	4096	3344.36	2896.31	2590.53	579.26	183.17
Gaussian Mechanism ($\delta = 10^{-6}$) ϵ	1918.24	1354.08	1107.57	959.18	857.76	191.82	60.66

Table 2: Differential privacy risk for different distortion values

Expression Classification	Original Data		D = 1		D = 3		D = 5	
	Male	Female	Male	Female	Male	Female	Male	Female
False Positive Rate	0.04	0.14	0.1	0.18	0.18	0.16	0.16	0.14
False Negative Rate	0.16	0.02	0.2	0.08	0.26	0.12	0.24	0.24

Table 3: Error rates for expression classification using representation learned by FNND

Expression Classification	Original Data		D = 1		D = 3		D = 5	
	Male	Female	Male	Female	Male	Female	Male	Female
False Positive Rate	0.04	0.14	0.04	0.16	0.06	0.12	0.08	0.16
False Negative Rate	0.16	0.02	0.2	0.08	0.2	0.14	0.18	0.16

Table 4: Error rates for expression classification using representation learned by TCNND

To demonstrate the effectiveness of the learned GAP schemes, we compare the gender classification accuracy of the learned GAP schemes with adding uniform or Laplace noise. Figure 5a shows that for the same distortion, the learned GAP schemes achieve much lower gender classification accuracy than using uniform or Laplace noise. Furthermore, the estimated mutual information $\hat{I}(\hat{X}; S)$ normalized by $\hat{I}(X; S)$ also decreases as the distortion increases (Figure 5b).

To evaluate the influence of GAP on other non-sensitive variable (Y) classification tasks, we train another CNN (see Figure 18) to perform facial expression classification on datasets processed by different decorrelation schemes. The trained model is then tested on the original test data. In Figure 5a, we observe that the expression classification accuracy decreases gradually as the distortion increases. Even for a large distortion value (5 per image), the expression classification accuracy only decreases by 10%. Furthermore, the estimated normalized mutual information $\hat{I}(\hat{X}; Y)/\hat{I}(X; Y)$ decreases much slower than $\hat{I}(\hat{X}; S)/\hat{I}(X; S)$ as the distortion increases (Figure 5b).

Table 3 and 4 present different error rates for the facial expression classifiers trained using data representations created by different decorrelator architectures. We observe that as distortion increases, the error rates difference for different sensitive groups decrease. This implies the classifier’s decision is less biased to the sensitive variables when trained using the processed data. When $D = 5$, the differences are already very small. Furthermore, we notice that the FNND architecture performs better in enforcing fairness but suffers from higher error rate. The images processed by FNND is shown in Figure 6. The decorrelator changes mostly eyes, nose, mouth, beard, and hair.

5.2 Illustration of Results for HAR Dataset

Figure 7a illustrates the activity and identity classification accuracy for different values of distortion. The adversary’s sensitive variable (identity) classification accuracy decreases progressively as the distortion increases. When the distortion is small ($D = 2$), the adversary’s classification accuracy is already around 27%. If we increase the distortion to 8, the classification accuracy further decreases to 3.8%. Figure 7a depicts that even for a large distortion value ($D = 8$), the

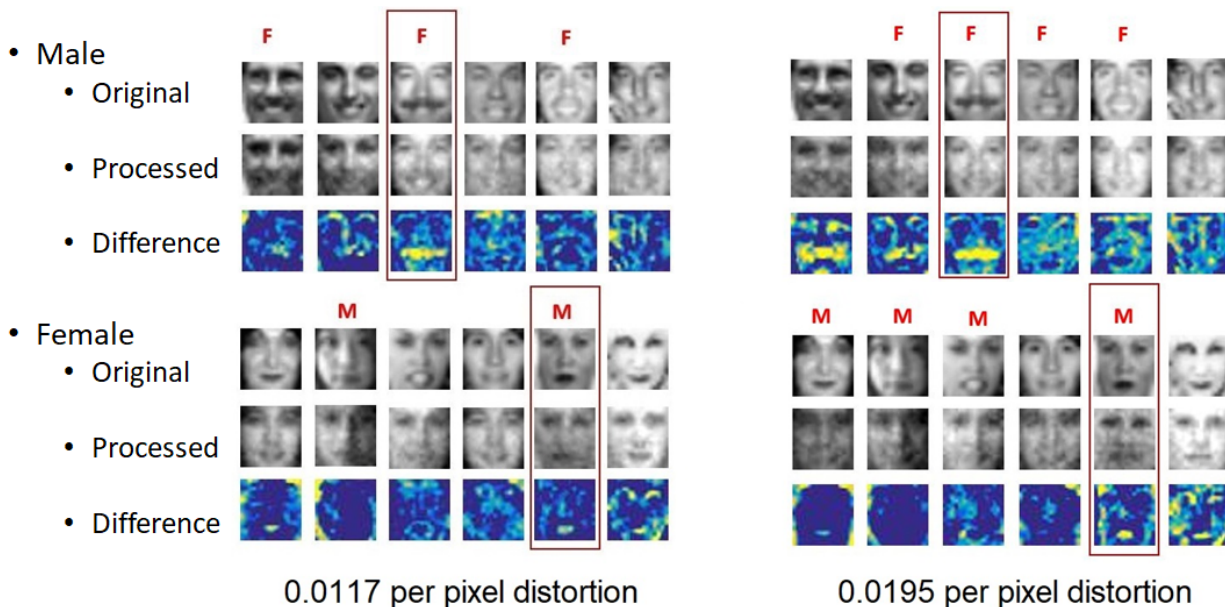
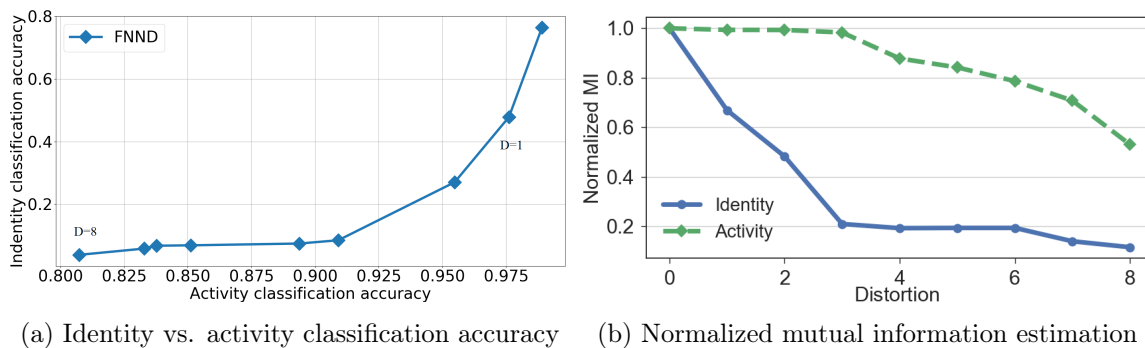


Figure 6: Perturbed images with different per pixel distortion using FNND

activity classification accuracy only decreases by 18% at most. Furthermore, Figure 7b shows that the estimated normalized mutual information also decreases as the distortion increases.



(a) Identity vs. activity classification accuracy (b) Normalized mutual information estimation

Figure 7: Censoring/fairness-utility tradeoff and mutual information estimation for HAR

5.3 Illustration of Results for UCI Adult Dataset

For the UCI Adult dataset with both categorical and continuous features as shown in Table 5, we consider two cases: (i) in Case I, the sensitive variable S is gender, which is either male or female, and (ii) in Case II, the sensitive variable S is the couple of gender and relationship, which has 12 possibilities. In both cases, the target variable Y is salary, which is either $> 50K$ or $\leq 50K$. For the binary target variable, the two values of the fair statistic Δ_{DemP} in (13) are the same, and for simplification, we use Δ_{DemP} to indicate the value.

Case I: Binary Sensitive Feature.

Fig. 8 illustrates the censoring-utility tradeoff (CUT) and fairness-utility tradeoff (FUT) for the GAP X_r generated under two scenarios: (i) the encoder $g(\cdot)$ of the original GAP framework in (6) takes only the non-sensitive features X as the input and (2) the encoder $g(\cdot)$ in (6) takes both X

Case I	Feature	Description	Case II
Y	salary	2-salary intervals: $> 50K$ and $\leq 50K$	Y
S	gender	2 classes: male and female	S
X	relationship	6 classes of family relationships (e.g., wife and husband)	X
	age	9-age intervals: 18 – 25, 25 – 30, 30 – 35, ..., 60 – 65	
	workclass	8 types of employer	
	education	16 levels of the highest achieved education	
	marital-status	7 classes of marital status	
	occupation	14 types of occupation	
	race	5 classes	
	native-country	41 countries of origin	
	capital-gain	Recorded capital gain; (continuous)	
	capital-loss	Recorded capital loss; (continuous)	
	hours-per-week	Worked hours per week; (continuous)	
education-num	Numerical version of education; (continuous)		

Table 5: Features of the UCI Adult dataset

and S as the input.

From Fig. 8a, we observe that: (i) while the classification accuracy of the sensitive variable (gender) is about 66% and decreases about 20% from the baseline, i.e., accuracy obtained from the original data, the classification accuracy of the target variable (salary) is above 82% and only decreases 2.5% from its baseline. Note that 66% is probability of male in the original testing data and indicates a random guess of gender. Therefore, the GAP X_r hides the information about gender pretty well while maintains the information about salary; (ii) only in the high utility region, where the accuracy of salary is no less than 72.5%, to take both S and X as the input of the encoder $g(\cdot)$ have a small advantage over only feeding X into the encoder $g(\cdot)$. Specifically, given the same accuracy of the sensitive variable (gender), the accuracy of the target variable (salary) is at most 0.3% higher. From this, we can know that gender is highly related to salary in this dataset and the GAP framework is doing the right job by preferentially hiding the sensitive information gender.

From Fig. 8b, we observe that (i) as the accuracy of salary decreases, the fairness statistic Δ_{DemP} becomes smaller. While the Δ_{DemP} is almost 0, the accuracy of salary is above 79% and the FUT of the GAP X_r has a linear relationship. Therefore, the GAP framework is effective to approach perfect demographic parity; (ii) the GAP X_r generated from either X or (S, X) leads to a similar FUT. Therefore, to generate X_r by feeding X or (S, X) into the encoder $g(\cdot)$ results in similar censoring/fairness guarantee for given utility, which verifies that the GAP framework is efficient in generating a censored/fair representation *w.r.t.* the sensitive feature gender.

Case II: Non-binary Sensitive Feature. Figs. 9 and 10 illustrate the censoring/fairness-utility tradeoffs for Case II with both gender and relationship as the sensitive features.

Fig. 9 shows the CUTs of the GAP X_r in hiding gender and/or relationship while maintains the information about salary. From Fig. 9, we observe that while the classification accuracy of the target variable (salary) is above 79%, the classification accuracies of gender and/or relationship are about 66% (as shown in Fig. 9a), 45% (as shown in Fig. 9b) and 41% (as shown in Fig. 9c), respectively. Note that the probabilities of male, husband, and the combination (male, husband) is 66%, 40% and 40%, respectively, in the original testing data, and therefore, when the classification accuracy of salary is about 79%, the corresponding classification accuracy for gender, relationship, and combination (gender, relationship) indicate a random guess with known prior. Therefore, the GAP X_r works pretty well in hiding multiple sensitive information separately or jointly. On the

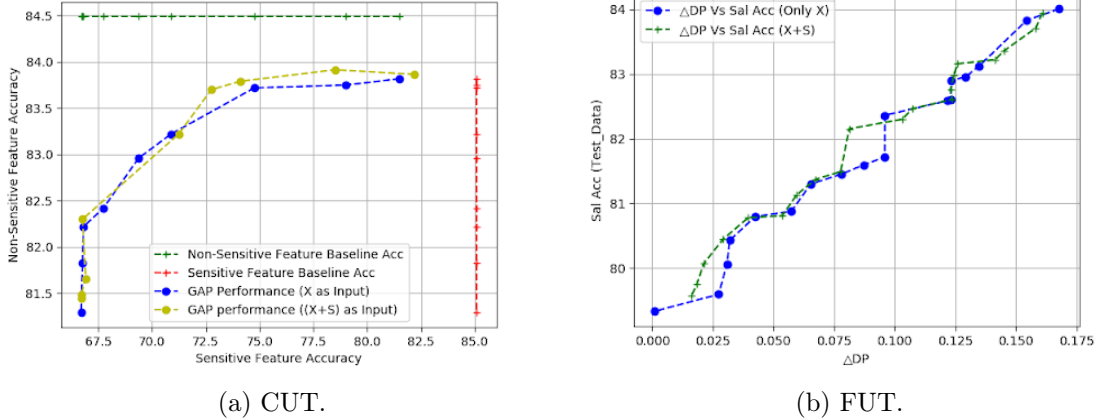


Figure 8: Censoring/fairness-utility tradeoffs for Case I of UCI Adult. Note that in Fig. 8a we use the classification accuracy for the original testing dataset (only using the non-sensitive feature X) as the baseline. The green and red lines denote the baselines for the target variable (salary) and the sensitive variable (gender), respectively; in Fig. 8b, the value of Δ_{DemP} for the original testing data is 0.2.

other hand, to have the flexibility of hiding the other sensitive information, i.e., relationship, the cost is a reduce in utility for a given classification accuracy of gender. Compare the results in Figs. 8a and 9a, we can see that the drop of the classification accuracy of salary is at most 3% for any given accuracy of gender. Note that in Figs., 8a and 9a, the baselines, i.e., the accuracy of salary and gender, are different is because of the lack of relationship in the feature variable X for Case II compared to Case I.

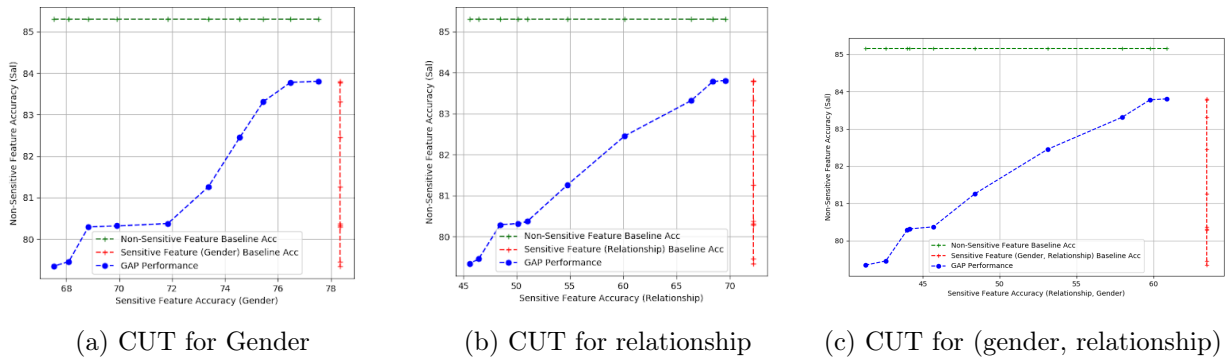


Figure 9: CUTs for Case II of UCI Adult. Note that we use the classification accuracy obtained from the original testing dataset as the baseline, which is denoted by the green and red lines for the target variable (salary) and the sensitive variable (gender or/and relationship), respectively.

Fig. 10 shows the FUTs of the GAP X_r in predicting salary. We observe that while the classification accuracy of salary is above 94% of the baseline (i.e., 85.15% the accuracy for the original testing dataset), the fairness statistic Δ_{DemP} (defined in (13)) is dropped to 25% for gender and about 34% for both relationship and the couple (relationship gender). Therefore, the GAP X_r works well in decorrelating the information of salary and the information of gender and relationship jointly and separately. From 10b, we observe that the value of Δ_{DemP} for the couple (relationship, gender) is almost the same as that for relationship. In addition, to compare the FUTs in Figs. 8b

and 10b, we can see that for given classification accuracy of salary, the Δ_{DemP} for gender in Case II can be about 0.05 (about 25% of the baseline 0.2) larger than that in Case I, which is the cost of providing fairness for relationship.

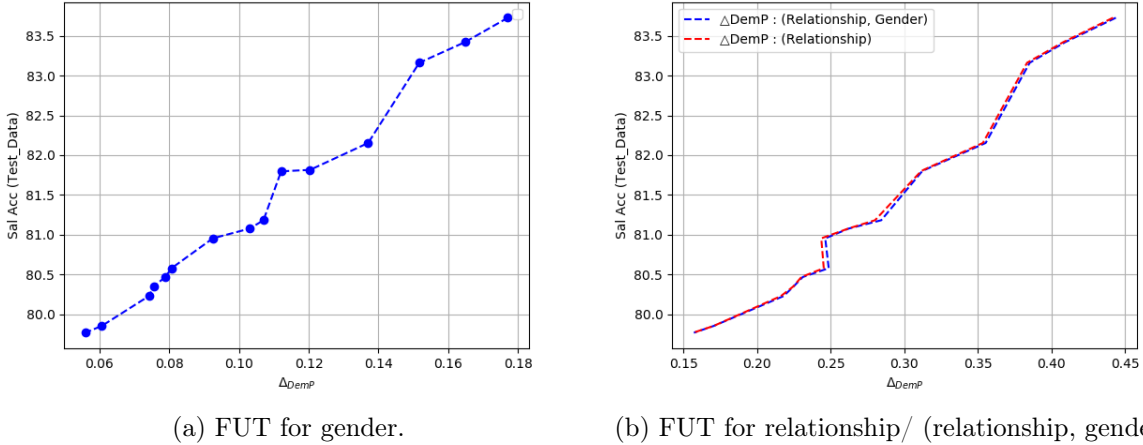


Figure 10: FUTs for Case II of UCI Adult. Note that in Fig. 10b, the red and blue lines are the fairness statistic Δ_{DemP} for relationship and (gender, relationship), respectively. For the original testing data, the value of Δ_{DemP} for gender, relationship and (gender, relationship) is 0.2, 0.438 and 0.443 , respectively.

5.4 Illustration of Results for UTKFace Dataset

We generate the GAP X_r , which is decorrelated from gender (the sensitive feature), for face images in the UTKFace dataset and show the effectiveness of X_r by illustrating its censoring/fairness-utility tradeoffs in two downstream applications: ethnicity classification and age regression. For the two application, the supports of the target variable Y are $\mathcal{Y} = \{\text{White, Black, Asian, Indian}\}$ and $\mathcal{Y} = \{i \in \mathbb{Z} : 10 \leq i \leq 65\} = [10, 65]$, respectively. We use the maximal value of the demographic parity measure defined in (13), i.e., $\Delta_{\text{DemP}} = \max_{y \in \mathcal{Y}}$, as the fairness indicator.

Fig. 11 illustrates various-distorted GAP X_r for 16 typical faces in the UTKFace dataset. The 16 typical faces covers the 8 possible combination of 2 gender (male and female) and 4 ethnicity (White, Black, Asian and Indian) and includes young, adult and old faces. From 11, we can observe (i) for a small per-pixel distortion (e.g., 0.003), the distinguished features of gender like lipstick are smoothed out in the GAP; and (ii) as a higher per-pixel distortion allowed (e.g., 0.006), the GAP approaches a face with an opposite gender; (iii) however, when the per-pixel distortion is too large (e.g., 0.01), the GAP tends to be too blurred to show the face contour and clear five sense organs.

Figs. 12a and 13 show the CUTs of the GAP X_r for the ethnicity classification and age regression, respectively. In Fig. 12a, while the classification accuracy of gender is about 62% and decreases about 35% from the baseline, i.e., accuracy obtained from the original testing data, the classification accuracy of ethnicity is above 74% and only decreases 14% from its baseline. Note that in the original testing data, the highest marginal probability for gender and ethnicity are 54.6% (the probability of male) and 43.2% (the probability of White), respectively. Therefore, the 62% classification accuracy of gender is only better than a random guess by 7.4% while the 74% classification accuracy of ethnicity is better than a random guess by 30.8%. Therefore, the GAP X_r hides the information about gender well while maintains the information about salary. For age regression, we use the mean absolute error (MAE), i.e., the average absolute difference between the predicted age and the true

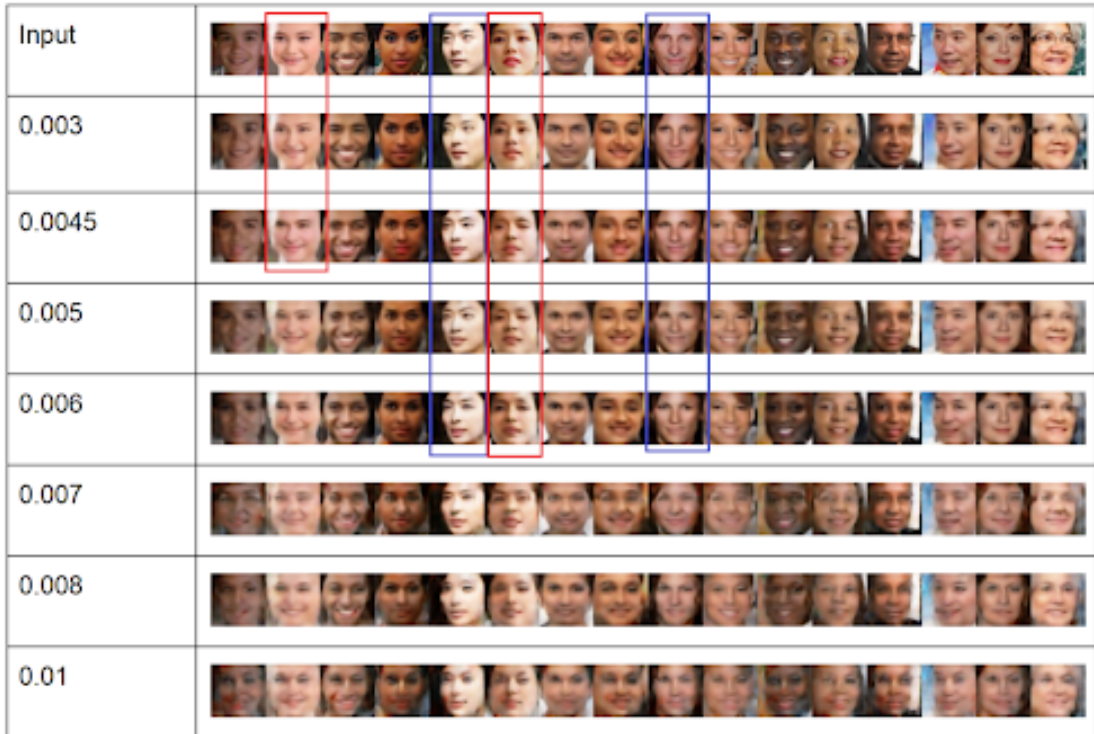


Figure 11: The GAP of face images under various per-pixel distortions for UTKFace. Note that the distortion is the per pixel distortion.

age, as the utility measure. In Fig. 13a, we observe that while the classification accuracy for gender is about 62%, which is 35% decrease from the baseline 94%, the increase in the MAE is 1.5 which is about 20% increase from the baseline 7.2. Fig. 13a shows the cumulative distribution function (CDF) of the difference between the true and predicted age for various distortions, from which we can see that the drop of the cumulative probability is at most 1%. Therefore, the GAP also does a good job in keeping the information about age and to limit the distortion of the representation is an efficient way for guaranteeing utilities of various applications.

Figs. 12b and 14 show the FUTs of the GAP X_r in ethnicity classification and age regression, respectively. In Fig. 12b, we observe that to achieve about 86% of the baseline, i.e., the classification accuracy of ethnicity obtained from the original testing dataset, the GAP X_r reduces the Δ_{DemP} , the maximal value of the demographic parity measure (defined in (13)) over the four ethnicity, to 0.03 which is only 20% of the $\Delta_{\text{DemP}} = 0.14$ on the original testing data. Therefore, the GAP does a good job in approaching demographic parity fairness while maintain the utility for ethnicity classification. Table 6 shows the decrease of each of the demographic parity measure for the four ethnicity as the distortion increases. In fig. 14a, while preserving 86% of the utility baseline, the Δ_{DemP} , i.e., the maximal value of demographic parity measure over the 56 ages, to 0.015 which is less than 33% of the $\Delta_{\text{DemP}} = 0.046$ on the original testing data. Fig. 14b shows the demographic parity measure $\Delta_{\text{DemP}}(y)$, $y \in [10, 65]$, for various distortions, from which we observe that when the pixel distortion is 0.01, even though the $\Delta_{\text{DemP}} = 0.015$, for 17 different ages, $\Delta_{\text{DemP}}(y) = 0$. That is, the prediction of these 17 different ages is completely independent of gender (the sensitive information) and demographic parity is achieved for those predictions.

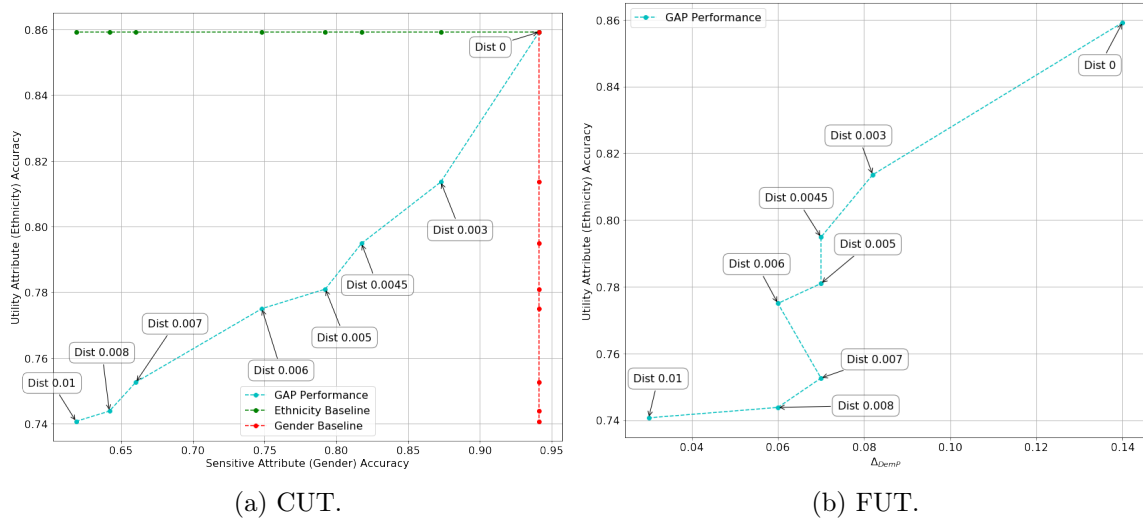


Figure 12: The tradeoffs for ethnicity classification on the UTKFace dataset. Note that in Fig. 12b, the x-axis is the maximal value of demographic parity measure in (13) over the four ethnicity.

Distortion	0	0.003	0.0045	0.005	0.006	0.007	0.008	0.01
$\Delta_{\text{DemP}}(\text{white})$	0.061	0.055	0.04	0.03	0.03	0.02	0.02	0.01
$\Delta_{\text{DemP}}(\text{black})$	0.109	0.021	0.02	0.05	0.03	0.05	0.03	0.03
$\Delta_{\text{DemP}}(\text{Asian})$	0.14	0.082	0.07	0.07	0.06	0.07	0.06	0.03
$\Delta_{\text{DemP}}(\text{Indian})$	0.031	0.006	0.01	0	0.01	0	0.01	0.01

Table 6: The demographic parity fairness (indicated by $\Delta_{\text{DemP}}(\cdot)$) of ethnicity classification on the UTKFace dataset.

6 Conclusion

We have introduced a novel adversarial learning framework for creating private/fair representations of the data with verifiable guarantees. GAP allows the data holder to learn the decorrelation scheme directly from the dataset (to be published) without requiring access to dataset statistics. Under GAP, finding the optimal decorrelation scheme is formulated as a game between two players: a generative decorrelator and an adversary. We have shown that for appropriately chosen loss functions, GAP can provide guarantees against strong information-theoretic adversaries, such as MAP and MI adversaries. It can also enforce fairness, quantified via demographic parity by using the log-loss function. We have also validated the performance of GAP on Gaussian mixture models and real datasets. There are several fundamental questions that we seek to address. An immediate one is to develop techniques to rigorously benchmark data-driven results for large datasets against computable theoretical guarantees. More broadly, it will be interesting to investigate the robustness and convergence speed of the decorrelation schemes learned in a data-driven fashion. In this paper, we connect our objective function in GAP with demographic parity. Since there is no single metric for fairness, this leaves room for designing objective functions that link to other fairness metrics such as equalized odds and equal opportunity.

Acknowledgments

We would like to acknowledge support for this project from the National Science Foundation via grants CCF-1422358, CCF-1350914, CIF-1815361 and CIF-1901243. We would also like to thank Prof. Ram Rajagopal and Xiao Chen at Stanford for their help with estimating mutual information

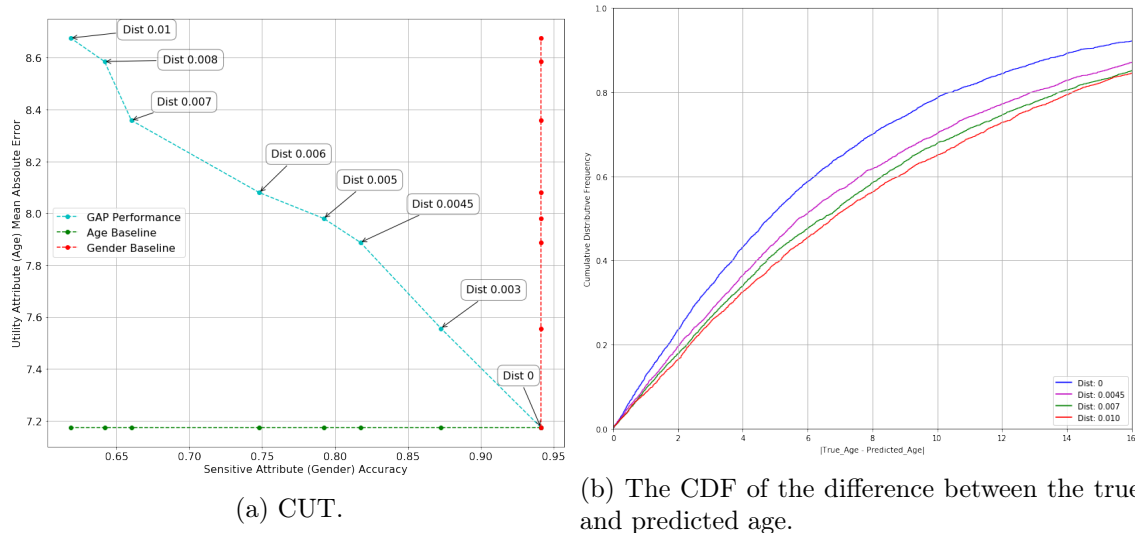
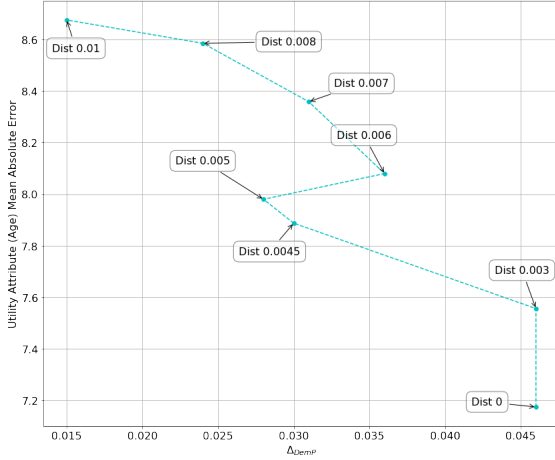
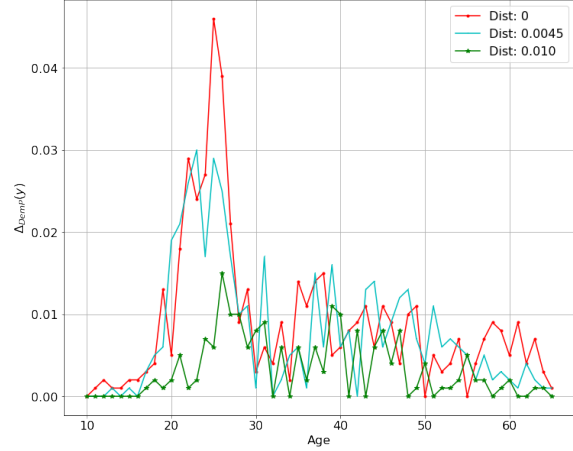


Figure 13: The tradeoffs and performance for age regression on the UTKFace dataset. Note that the distortion is the per pixel distortion.

for the GENKI and HAR datasets, and would like to thank Maunil Vyas, Mit Patel and Harshit Laddha at ASU for their help with the experiments on the UCI Adult and UTKFace datasets.



(a) FUT.



(b) The demographic parity measure for various distortions.

Figure 14: The achieved fairness for age regression on the UTKFace dataset. Note that in Fig. 14a, the x-axis is the maximal value of demographic parity measure in (13) over the 56 ages.

A Proof of Theorem 1

An encoder $g(X)$ that satisfies demographic parity ensures that X_r is independent of S , i.e., the mutual information $I(S; X_r) = 0$. Further, the downstream learning algorithm acts only on X_r to predict \hat{Y} ; combining these, we have that, $(S, X) - X_r - \hat{Y}$ form a Markov chain. From Definition 3, since X_r is independent of S , $I(S; X_r) = 0$. From the data processing inequality and non-negativity of mutual information, we have that,

$$0 \leq I(S; \hat{Y}) \leq I(S; X_r) = 0. \quad (14)$$

Therefore, S is independent of \hat{Y} , and thus, from Definition 1, \hat{Y} satisfies demographic parity w.r.t. S .

Note that S can be collection of sensitive features. From the fact $I(S; X_r) = 0$ as well as the chain rule and non-negativity of mutual information, we have $I(X_r; S_t) = 0$ for any subset of features $S_t \subset S$. Therefore, \hat{Y} satisfies demographic parity w.r.t. any subset of features in S .

B Theoretical Results of GAP

Our GAP framework places no restrictions on the adversary. Indeed, different loss functions and decision rules lead to different adversarial models. In what follows, we will discuss a variety of loss functions under hard and soft decision rules, and show how our GAP framework provides censoring guarantee against various adversaries. We will also show that we can obtain a continuous interpolation between a hard-decision adversary under 0-1 loss function and a soft-decision adversary under log-loss function using the α -loss function.

Hard Decision Rules. When the adversary adopts a hard decision rule, $h(g(X))$ is an estimate of S . Under this setting, we can choose $\ell(h(g(X)), S)$ in a variety of ways. For instance, if S is continuous, the adversary can attempt to minimize the difference between the estimated and true sensitive variable values. This can be achieved by considering a squared loss function

$$\ell(h(g(X)), S) = (h(g(X)) - S)^2, \quad (15)$$

which is known as the ℓ_2 loss. In this case, one can verify that the adversary’s optimal decision rule is $h^* = \mathbb{E}[S|g(X)]$, which is the conditional mean of S given $g(X)$. Furthermore, under the adversary’s optimal decision rule, the minimax problem in (6) simplifies to

$$\min_{g(\cdot)} -\text{mmse}(S|g(X)) = -\max_{g(\cdot)} \text{mmse}(S|g(X)),$$

subject to the distortion constraint. Here $\text{mmse}(S|g(X))$ is the resulting minimum mean square error (MMSE) under $h^* = \mathbb{E}[S|g(X)]$. Thus, under the ℓ_2 loss, GAP provides censoring guarantees against an MMSE adversary. On the other hand, when S is discrete (e.g., age, gender, political affiliation, etc), the adversary can attempt to maximize its classification accuracy. This is achieved by considering a 0-1 loss function [Nguyen and Sanner, 2013] given by

$$\ell(h(g(X)), S) = \begin{cases} 0 & \text{if } h(g(X)) = S \\ 1 & \text{otherwise} \end{cases}. \quad (16)$$

In this case, one can verify that the adversary’s optimal decision rule is the *maximum a posteriori probability* (MAP) decision rule: $h^* = \text{argmax}_{s \in \mathcal{S}} P(s|g(X))$, with ties broken uniformly at random. Moreover, under the MAP decision rule, the minimax problem in (6) reduces to

$$\min_{g(\cdot)} -(1 - \max_{s \in \mathcal{S}} P(s, g(X))) = \min_{g(\cdot)} \max_{s \in \mathcal{S}} P(s, g(X)) - 1, \quad (17)$$

subject to the distortion constraint. Thus, under a 0-1 loss function, the GAP formulation provides censoring guarantees against a MAP adversary.

Soft Decision Rules. Instead of a *hard decision* rule, we can also consider a broader class of *soft decision* rules where $h(g(X))$ is a distribution over \mathcal{S} ; i.e., $h(g(X)) = P_h(s|g(X))$ for $s \in \mathcal{S}$. In this context, we can analyze the performance under a log-loss

$$\ell(h(g(X)), s) = \log \frac{1}{P_h(s|g(X))}. \quad (18)$$

In this case, the objective of the adversary simplifies to

$$\max_{h(\cdot)} -\mathbb{E}[\log \frac{1}{P_h(s|g(X))}] = -H(S|g(X)),$$

and that the maximization is attained at $P_h^*(s|g(X)) = P(s|g(X))$. Therefore, the optimal adversarial decision rule is determined by the true conditional distribution $P(s|g(X))$, which we assume is known to the data holder in the game-theoretic setting. Thus, under the log-loss function, the minimax optimization problem in (6) reduces to

$$\min_{g(\cdot)} -H(S|g(X)) = \min_{g(\cdot)} I(g(X); S) - H(S),$$

subject to the distortion constraint. Thus, under the log-loss in (18), GAP is equivalent to using MI as the privacy metric [Calmon and Fawaz, 2012].

The 0-1 loss captures a strong guessing adversary; in contrast, log-loss or information-loss models a belief refining adversary.

B.1 Proof of Theorem 2

In (6), the output of the optimal encoder $g^*(X)$ is the GAP of the original features X , i.e., $X_r = g^*(X) = \text{argmin}_{g(\cdot)} \max_{h(\cdot)} -\mathbb{E}[\ell(h(g(X)); S)]$. Let h^* be the corresponding optimal adversarial

strategy i.e., $h_{g^*}^* = \operatorname{argmin}_h \mathbb{E}[\ell(h(X_r), S)]$. For sufficient large distortion bound D , X_r can be arbitrarily distorted from X and $g(\cdot)$ can be any mapping from X to X_r . Therefore, we can get ride of the distortion constraint in (6) and have

$$-\mathbb{E}[\ell(h_{g^*}^*(X_r); S)] = -\max_{g(\cdot)} \min_{h(\cdot)} \mathbb{E}[\ell(h(g(X)); S)] \quad (19)$$

$$= -\max_{g(\cdot)} \mathbb{E}[\ell(h_g^*(g(X)); S)], \quad (20)$$

$$\leq -\mathbb{E}[\ell(h_g^*(g(X)); S)], \quad (21)$$

$$(22)$$

where $g(X)$ is any (randomized) mapping of X . That is, the GAP X_r satisfies the inequality in (4). Thus, for sufficiently large distortion bound D , the GAP X_r generated from the formulation in (6) is censored *w.r.t.* the sensitive variable S against a learning adversary $h(\cdot)$ captured by a loss function $\ell(h(X_r), S)$.

B.2 Proof of Proposition 1

Consider the α -loss function [Liao et al., 2018]

$$\ell(h(g(X)), s) = \frac{\alpha}{\alpha - 1} \left(1 - P_h(s|g(X))^{1 - \frac{1}{\alpha}} \right), \quad (23)$$

for any $\alpha > 1$. Denote $H_\alpha^A(S|g(X))$ as the Arimoto conditional entropy of order α . Due to that α -loss is convex in $P_h(s|g(X))$, by using Karush–Kuhn–Tucker (KKT) conditions, we show that

$$\max_{h(\cdot)} -\mathbb{E} \left[\frac{\alpha}{\alpha - 1} \left(1 - P_h(s|g(X))^{1 - \frac{1}{\alpha}} \right) \right] = \frac{\alpha}{1 - \alpha} \left(1 - \exp \left(\frac{1 - \alpha}{\alpha} H_\alpha^A(S|g(X)) \right) \right)$$

which is achieved by a ‘ α -tilted’ conditional distribution

$$P_h^*(s|g(X)) = \frac{P(s|g(X))^\alpha}{\sum_{s \in \mathcal{S}} P(s|g(X))^\alpha}.$$

Under this choice of a decision rule, the objective of the minimax optimization in (6) reduces to

$$\min_{g(\cdot)} -H_\alpha^A(S|g(X)). \quad (24)$$

B.3 Proof of Corollary 1

For large α ($\alpha \rightarrow \infty$), this loss approaches that of the 0-1 (MAP) adversary in the limit. As α decreases, the convexity of the loss function encourages the estimator \hat{S} to be probabilistic, as it increasingly rewards correct inferences of lesser and lesser likely outcomes (in contrast to a hard decision rule by a MAP adversary of the most likely outcome) conditioned on the revealed data. As $\alpha \rightarrow 1$, (23) yields the logarithmic loss, and the optimal belief $P_{\hat{S}}$ is simply the posterior belief. Therefore, using α -loss, we can obtain a continuous interpolation between a hard-decision adversary under 0-1 loss ($\alpha \rightarrow \infty$) and a soft-decision adversary under log-loss function ($\alpha \rightarrow 1$).

B.4 Proof of Theorem 3

For any fixed classifier g , the optimal adversarial strategy in (6) is

$$h^*(g(X)) = \arg \max_{h(\cdot)} -\mathbb{E}[\ell(h(g(X)), S)]. \quad (25)$$

When α -loss is used, from Proposition. 1 we have that for $\alpha \geq 1$, the optimal adversarial strategy is given by

$$h^*(g(X), S) = \frac{P(s|g(X))^\alpha}{\sum_{s' \in \mathcal{S}} P(s'|g(X))^\alpha}, \quad (26)$$

for any $s \in \mathcal{S}$, and the corresponding expected α -loss is given by

$$\mathbb{E}[\ell(h(g(X)), S)] = \begin{cases} \frac{\alpha}{\alpha-1} (1 - \exp(-\frac{1-\alpha}{\alpha} H_\alpha^A(S|g(X)))) , & \alpha > 1 \\ H(S|g(X)), & \alpha = 1. \end{cases} \quad (27)$$

Therefore, the optimization in (6) can be simplified to

$$\min_{g(\cdot)} -H_\alpha^A(S|g(X)), \quad (28a)$$

$$\text{s.t. } \mathbb{E}[d(g(X), X)] \leq D \quad (28b)$$

where $H_\alpha^A(S|g(X))$ is the Arimoto conditional entropy of order α . Note that as α tends to 1, it simplifies to Shannon entropy [Verdu, '15]. From the non-negativity of Arimoto mutual information, we know that

$$H_\alpha^A(S|g(X)) \leq H_\alpha^A(S) \quad (29)$$

with equality if and only if $g(X)$ is independent of S , which is exactly the requirement of demographic parity. Thus, as the distortion bound D in (28) increases, the GAP formulation in (28) will approach ideal demographic parity by enforcing $H_\alpha^A(S|g(X)) = H_\alpha^A(S)$.

B.5 Proof of Theorem 2

For any fixed classifier \tilde{g} , the optimal adversarial strategy in (8) is

$$h^*(\tilde{g}(S, X), Y) = \arg \max_{h(\cdot)} -\mathbb{E}[\ell(h(\tilde{g}(S, X), Y), S)]. \quad (30)$$

When α -loss is used, from Proposition. 1 we have that for $\alpha \geq 1$, the optimal adversarial strategy is given by

$$h^*(\tilde{g}(S, X), Y) = \frac{P(s|\tilde{g}(S, X), Y)^\alpha}{\sum_{s' \in \mathcal{S}} P(s'|\tilde{g}(S, X), Y)^\alpha}, \quad (31)$$

for any $s \in \mathcal{S}$, and the corresponding expected α -loss is given by

$$\mathbb{E}[\ell(h(\tilde{g}(S, X), Y), S)] = \begin{cases} \frac{\alpha}{\alpha-1} (1 - \exp(-\frac{1-\alpha}{\alpha} H_\alpha^A(S|\tilde{g}(S, X), Y))) , & \alpha > 1 \\ H(S|\tilde{g}(S, X), Y), & \alpha = 1. \end{cases} \quad (32)$$

Therefore, the optimization in (8) can be simplified to

$$\min_{\tilde{g}(\cdot)} -H_{\alpha}^{\text{A}}(S|\tilde{g}(S, X), Y), \quad (33\text{a})$$

$$\text{s.t. } \mathbb{E}[\ell(\tilde{g}(S, X), Y)] \leq L \quad (33\text{b})$$

where $H_{\alpha}^{\text{A}}(S|\tilde{g}(S, X), Y)$ is the Arimoto conditional entropy of order α . Note that as α tends to 1, it simplifies to Shannon entropy [Verdu, '15].

From the non-negativity of Arimoto mutual information, we know that

$$H_{\alpha}^{\text{A}}(S|\tilde{g}(S, X), Y) \leq H_{\alpha}^{\text{A}}(S|Y) \quad (34)$$

with equality if and only if $\tilde{g}(S, X)$ is independent of S conditioning on Y , which is exactly the requirement of equalized odds. Thus, as the loss upper-bound L in (33) increases, the GAP formulation in (33) will approach ideal equalized odds of $\tilde{g}(S, X)$ respect to Y and S by enforcing $H_{\alpha}^{\text{A}}(S|\tilde{g}(S, X), Y) = H_{\alpha}^{\text{A}}(S|Y)$.

C Alternate Minimax Algorithm

In this section, we present the alternate minimax algorithm to learn the GAP scheme from a dataset. The alternating minimax censoring preserving algorithm is presented in Algorithm 1. To incorporate the distortion constraint into the learning algorithm, we use the *penalty method* [Lillo et al., 1993] and *augmented Lagrangian method* [Eckstein and Yao, 2012] to replace the constrained optimization problem by a series of unconstrained problems whose solutions asymptotically converge to the solution of the constrained problem. Under the penalty method, the unconstrained optimization problem is formed by adding a penalty to the objective function. The added penalty consists of a penalty parameter ρ_t multiplied by a measure of violation of the constraint. The measure of violation is non-zero when the constraint is violated and is zero if the constraint is not violated. Therefore, in Algorithm 1, the constrained optimization problem of the decorrelator can be approximated by a series of unconstrained optimization problems with the loss function

$$\ell(\theta_p^t, \theta_a^{t+1}) = -\frac{1}{M} \sum_{i=1}^M \ell(h(g(x_{(i)}; \theta_p^t); \theta_a^{t+1}), s_{(i)}) + \rho_t (\max\{0, \frac{1}{M} \sum_{i=1}^M d(g(x_{(i)}; \theta_p^t), x_{(i)}) - D\})^2, \quad (35)$$

where ρ_t is a penalty coefficient which increases with the number of iterations t . For convex optimization problems, the solution to the series of unconstrained problems will eventually converge to the solution of the original constrained problem [Lillo et al., 1993].

The augmented Lagrangian method is another approach to enforce equality constraints by penalizing the objective function whenever the constraints are not satisfied. Different from the penalty method, the augmented Lagrangian method combines the use of a Lagrange multiplier and a quadratic penalty term. Note that this method is designed for equality constraints. Therefore, we introduce a slack variable δ to convert the inequality distortion constraint into an equality constraint. Using the augmented Lagrangian method, the constrained optimization problem of the decorrelator can be replaced by a series of unconstrained problems with the loss function given by

$$\begin{aligned} \ell(\theta_p^t, \theta_a^{t+1}, \delta) = & -\frac{1}{M} \sum_{i=1}^M \ell(h(g(x_{(i)}; \theta_p^t); \theta_a^{t+1}), s_{(i)}) + \frac{\rho_t}{2} \left(\frac{1}{M} \sum_{i=1}^M d(g(x_{(i)}; \theta_p^t), x_{(i)}) + \delta - D \right)^2 \\ & - \lambda_t \left(\frac{1}{M} \sum_{i=1}^M d(g(x_{(i)}; \theta_p^t), x_{(i)}) + \delta - D \right), \end{aligned} \quad (36)$$

where ρ_t is a penalty coefficient which increases with the number of iterations t and λ_t is updated according to the rule $\lambda_{t+1} = \lambda_t - \rho_t \left(\frac{1}{M} \sum_{i=1}^M d(g(x_{(i)}; \theta_p^t), x_{(i)}) + \delta - D \right)$. For convex optimization problems, the solution to the series of unconstrained problems formulated by the augmented Lagrangian method also converges to the solution of the original constrained problem [Eckstein and Yao, 2012].

C.1 Proof of Theorem 4

Since $\mathbb{E}_{X, \hat{X}}[d(\hat{X}, X)] = \mathbb{E}_{X, \hat{X}}\|X - \hat{X}\|^2 = \mathbb{E}\|Z + \beta\|^2 = \|\beta\|^2 + \text{tr}(\Sigma_p)$, the distortion constraint implies that $\|\beta\|^2 + \text{tr}(\Sigma_p) \leq D$. Let us consider $\hat{X} = X + Z + \beta$, where $\beta \in \mathbb{R}$ and Σ_p is a diagonal covariance whose diagonal entries is given by $\{\sigma_{p_1}^2, \dots, \sigma_{p_m}^2\}$. Given the MAP adversary's optimal inference accuracy in (10), the objective of the decorrelator is to

$$\begin{aligned} \min_{\beta, \Sigma_p} P_d^{(G)} \quad (37) \\ \text{s.t.} \quad \|\beta\|^2 + \text{tr}(\Sigma_p) \leq D. \end{aligned}$$

Define $\frac{1-q}{q} = \eta$. The gradient of $P_d^{(G)}$ w.r.t. α is given by

$$\frac{\partial P_d^{(G)}}{\partial \alpha} = \tilde{p} \left(-\frac{1}{\sqrt{2\pi}} e^{-\frac{(-\frac{\alpha}{2} + \frac{1}{\alpha} \ln \eta)^2}{2}} \right) \left(-\frac{1}{2} - \frac{1}{\alpha^2} \ln \eta \right) \quad (38)$$

$$\begin{aligned} &+ (1 - \tilde{p}) \left(-\frac{1}{\sqrt{2\pi}} e^{-\frac{(-\frac{\alpha}{2} - \frac{1}{\alpha} \ln \eta)^2}{2}} \right) \left(-\frac{1}{2} + \frac{1}{\alpha^2} \ln \eta \right) \\ &= \frac{1}{2\sqrt{2\pi}} \left(\tilde{p} e^{-\frac{(-\frac{\alpha}{2} + \frac{1}{\alpha} \ln \eta)^2}{2}} + (1 - \tilde{p}) e^{-\frac{(-\frac{\alpha}{2} - \frac{1}{\alpha} \ln \eta)^2}{2}} \right) \quad (39) \\ &+ \frac{\ln \eta}{\alpha^2 \sqrt{2\pi}} \left(\tilde{p} e^{-\frac{(-\frac{\alpha}{2} + \frac{1}{\alpha} \ln \eta)^2}{2}} - (1 - \tilde{p}) e^{-\frac{(-\frac{\alpha}{2} - \frac{1}{\alpha} \ln \eta)^2}{2}} \right). \end{aligned}$$

Note that

$$\frac{\tilde{p} e^{-\frac{(-\frac{\alpha}{2} + \frac{1}{\alpha} \ln \eta)^2}{2}}}{(1 - \tilde{p}) e^{-\frac{(-\frac{\alpha}{2} - \frac{1}{\alpha} \ln \eta)^2}{2}}} = \frac{\tilde{p}}{1 - \tilde{p}} e^{\frac{(-\frac{\alpha}{2} - \frac{1}{\alpha} \ln \eta)^2 - (-\frac{\alpha}{2} + \frac{1}{\alpha} \ln \eta)^2}{2}} = \frac{\tilde{p}}{1 - \tilde{p}} e^{\frac{2 \ln \eta}{2}} = \frac{\tilde{p}}{1 - \tilde{p}} e^{\ln \eta} = 1. \quad (40)$$

Therefore, the second term in (39) is 0. Furthermore, the first term in (39) is always positive. Thus, $P_d^{(G)}$ is monotonically increasing in α . As a result, the optimization problem in (37) is equivalent to

$$\begin{aligned} \min_{\beta, \Sigma_p} (2\mu)^T (\Sigma + \Sigma_p)^{-1} 2\mu \quad (41) \\ \text{s.t.} \quad \|\beta\|^2 + \text{tr}(\Sigma_p) \leq D. \end{aligned}$$

The objective function in (41) can be written as

$$2 \begin{bmatrix} \mu_1 & \mu_2 & \dots & \mu_m \end{bmatrix} \begin{bmatrix} \frac{1}{\sigma_1^2 + \sigma_{p_1}^2} & 0 & \dots & 0 \\ 0 & \frac{1}{\sigma_2^2 + \sigma_{p_2}^2} & \dots & 0 \\ \vdots & \vdots & \ddots & \vdots \\ 0 & 0 & \dots & \frac{1}{\sigma_m^2 + \sigma_{p_m}^2} \end{bmatrix} 2 \begin{bmatrix} \mu_1 \\ \mu_2 \\ \vdots \\ \mu_m \end{bmatrix} = \sum_{i=1}^m \frac{4\mu_i^2}{\sigma_i^2 + \sigma_{p_i}^2}.$$

Thus, the optimization problem in (41) is equivalent to

$$\begin{aligned} \min_{\beta, \sigma_{p_1}^2, \dots, \sigma_{p_m}^2} \quad & \sum_{i=1}^m \frac{\mu_i^2}{\sigma_i^2 + \sigma_{p_i}^2} \\ \text{s.t.} \quad & \|\beta\|^2 + \text{tr}(\Sigma_p) \leq D \\ & \sigma_{p_i}^2 \geq 0 \quad \forall i \in \{1, 2, \dots, m\}. \end{aligned} \quad (42)$$

Since a non-zero β does not affect the objective function but result in positive distortion, the optimal scheme satisfies $\beta = (0, \dots, 0)$. Furthermore, the Lagrangian of the above optimization problem is given by

$$L(\sigma_{p_1}^2, \dots, \sigma_{p_m}^2, \lambda) = \sum_{i=1}^m \frac{\mu_i^2}{\sigma_i^2 + \sigma_{p_i}^2} + \lambda_0 \left(\sum_{i=1}^m \sigma_{p_i}^2 - D \right) - \sum_{i=1}^m \lambda_i \sigma_{p_i}^2, \quad (43)$$

where $\lambda = \{\lambda_0, \dots, \lambda_m\}$ denotes the Lagrangian multipliers associated with the constraints. Taking the derivatives of $L(\sigma_{p_1}^2, \dots, \sigma_{p_m}^2, \lambda)$ with respect to $\sigma_{p_i}^2, \forall i \in \{1, \dots, m\}$, we have

$$\frac{\partial L(\sigma_{p_1}^2, \dots, \sigma_{p_m}^2, \lambda)}{\partial \sigma_{p_i}^2} = -\frac{\mu_i^2}{(\sigma_i^2 + \sigma_{p_i}^2)^2} + \lambda_0 - \lambda_i. \quad (44)$$

Notice that the objective function in (41) is decreasing in $\sigma_{p_i}^2, \forall i \in \{1, \dots, m\}$. Thus, the optimal solution $\sigma_{p_i}^{*2}$ satisfies $\sum_{i=1}^m \sigma_{p_i}^{*2} = D$. By the KKT conditions, we have

$$\left. \frac{\partial L(\sigma_{p_1}^2, \dots, \sigma_{p_m}^2, \lambda)}{\partial \sigma_{p_i}^2} \right|_{\sigma_{p_i}^2 = \sigma_{p_i}^{*2}, \lambda = \lambda^*} = -\frac{\mu_i^2}{(\sigma_i^2 + \sigma_{p_i}^{*2})^2} + \lambda_0^* - \lambda_i^* = 0. \quad (45)$$

Since $\lambda_i^*, i \in \{0, 1, \dots, m\}$ is dual feasible, we have $\lambda_i^* \geq 0, i \in \{0, 1, \dots, m\}$. Therefore

$$\lambda_0^* \geq \frac{\mu_i^2}{(\sigma_i^2 + \sigma_{p_i}^{*2})^2}.$$

If $\lambda_0^* > \frac{\mu_i^2}{\sigma_i^4}$, we have $\lambda_0^* > \frac{\mu_i^2}{(\sigma_i^2 + \sigma_{p_i}^{*2})^2}$. This implies $\lambda_i^* > 0$. Thus, by complementary slackness, $\sigma_{p_i}^{*2} = 0$. On the other hand, if $\lambda_0^* < \frac{\mu_i^2}{\sigma_i^4}$, we have $\sigma_{p_i}^{*2} > 0$. Furthermore, by the complementary slackness condition, $\lambda_i^* \sigma_{p_i}^{*2} = 0, \forall \sigma_{p_i}^{*2}$. This implies $\lambda_i^* = 0, \forall \sigma_{p_i}^{*2} > 0$. As a result, for all $\sigma_{p_i}^{*2} > 0$, we have

$$\frac{|\mu_i|}{\sqrt{\lambda_0^*}} = \sigma_i^2 + \sigma_{p_i}^{*2}. \quad (46)$$

Therefore, $\sigma_{p_i}^{*2} = \max\left\{\frac{|\mu_i|}{\sqrt{\lambda_0^*}} - \sigma_i^2, 0\right\} = \left(\frac{|\mu_i|}{\sqrt{\lambda_0^*}} - \sigma_i^2\right)^+$ with $\sum_{i=1}^m \sigma_{p_i}^{*2} = D$. Substitute this optimal solution into (10) with $\alpha = \sqrt{(2\mu)^T(\Sigma + \Sigma_p)^{-1}2\mu}$, we obtain the accuracy of the MAP adversary.

We observe that the when σ_i^2 is greater than some threshold $\frac{|\mu_i|}{\sqrt{\lambda_0^*}}$, no noise is added to the data on this dimension due to the high variance. When σ_i^2 is smaller than $\frac{|\mu_i|}{\sqrt{\lambda_0^*}}$, the amount of noise added to this dimension is proportional to $|\mu_i|$; this is intuitive since a large $|\mu_i|$ indicates the two conditionally Gaussian distributions are further away on this dimension, and thus, distinguishable. Thus, more noise needs to be added in order to reduce the MAP adversary's inference accuracy.

D Mutual Information Estimation

Our GAP framework offers a scalable way to find a (local) equilibrium in the constrained min-max optimization, under certain attacks (e.g. attacks based on a neural network). Yet the privatized data, through our approach, should be immune to any general attacks and ultimately achieving the goal of decreasing the correlation between the privatized data and the sensitive labels. Therefore we use the estimated mutual information to certify that the sensitive data indeed is protected via our framework.

We use the nearest k -th neighbor method [Kraskov et al., 2004] to estimate the entropy \hat{H} given by

$$\hat{H}(\hat{X}) = \psi(N) - \psi(k) + \log(c_d) + \frac{d}{N} \sum_{i=1}^N \log r_i \quad (47)$$

where r_i is the distance of the i -th sample \hat{x}_i to its k -th nearest neighbor, ψ is the digamma function, $c_d = \frac{\pi^{d/2}}{\Gamma(1+d/2)}$ in Euclidean norm, and N is the number of samples. Notice that \hat{X} is learned representation and S is the sensitive variable. Then, we calculate the mutual information using $\hat{I}(\hat{X}; S) = \hat{H}(\hat{X}) - \hat{H}(\hat{X}|S)$

For a binary sensitive variable, we can simplify the empirical MI to

$$\hat{I}(\hat{X}; S) = \hat{H}(\hat{X}) - (P(S=1)\hat{H}(\hat{X}|S=1) + P(S=0)\hat{H}(\hat{X}|S=0)), \quad (48)$$

where $P(S=1)$ and $P(S=0)$ can be approximated by the empirical probability.

One noteworthy difficulty is that \hat{X} usually lives in high dimensions (e.g. each image has 256 dimensions in GENKI dataset) which is almost impossible to calculate the empirical entropy based on raw data due to the sample complexity. Thus, we train a neural network that classifies the sensitive variable from the learned data representation to reduce the dimension of the data. We choose the layer before the softmax outputs (denoted by \hat{X}_f) to be the feature embedding that has a much lower dimension than original \hat{X} and also captures the information about the sensitive variable. We use \hat{X}_f as a surrogate of \hat{X} for estimating the entropy. The resulting approximate MI is

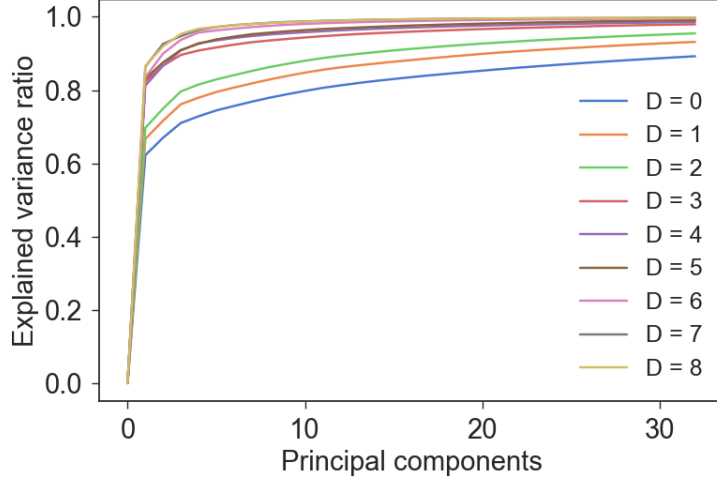
$$\begin{aligned} \hat{I}(\hat{X}_f; S) &= \hat{H}(\hat{X}_f) - \hat{H}(\hat{X}_f|S) \\ &= \hat{H}(\hat{X}_f) - (P(S=1)\hat{H}(\hat{X}_f|S=1) + P(S=0)\hat{H}(\hat{X}_f|S=0)). \end{aligned}$$

Following the same manner, the MI between the learned representation \hat{X} and the label Y is approximated by $\hat{I}(\hat{X}_f; Y)$, where \hat{X}_f is the feature embedding that represents a privatized image \hat{X} .

For the GENKI dataset, we construct a CNN initialized by two conv blocks, then followed by two fully connected (FC) layers, and lastly ended with two neurons having the softmax activations. In each conv block, we have a convolution layer consisting of filters with the size equals 3×3 and the stride equals 1, a 2×2 max-pooling layer with the stride equals 2, and a ReLU activation function. Those two conv blocks have 32 and 64 filters respectively. We flatten out the output of second conv block yielding a 256 dimension vector. The extracted features from the second conv layers is passed through the first FC layer with batch normalization and ReLU activation to get a 8-dimensional vector, followed with the second FC layer to output a 2 dimensional vector that applied with the softmax function. The aforementioned 8-dimensional vector is the feature embedding vector \hat{X}_f in our empirical MI estimation.

Estimating mutual information for HAR dataset has a slightly different challenge, as the size of the alphabet for the sensitive label (i.e. identity) is 30. Thus, it requires at least 30 neurons

prior to the output layer of the corresponding classification task. In fact we pose 128 neurons before the final softmax output layer in order to get a reasonably good classification accuracy. Using the 128-dimensional vector as our feature embedding to calculate mutual information is almost impossible due to the curse of dimensionality. Therefore, we apply Principal Component Analysis (PCA), shown in Figure 15, and pick the first 12 components to circumvent this issue. The resulting 12-dimensional vector is considered to be an approximate feature embedding that encapsulates the major information of the processed data.



(a) Top 32 principal components out of the 561 features with different distortion D

Figure 15: PCA for processed data in HAR

E Compute differential censoring risk for the Laplace and Gaussian noise adding mechanisms

In the local differential privacy setting, we consider the value of each pixel as the output of the query function. Since the pixel values of the GENKI dataset are normalized between 0 and 1, we can use the dimension of the image to bound the sensitivities for both Laplace mechanism and Gaussian mechanism. For the Laplace mechanism, let X and X' be two different image vectors. Since the value of X and X' in each dimension is between 0 and 1, $|X_i - X'_i| \leq 1$ for the i^{th} dimension. Thus, the L_1 sensitivity can be bounded by the dimension of the image d . Notice that the variance of the Laplace noise parameterized by λ is $2\lambda^2$. Since we are adding independent Laplace noise to each pixel, given the per image distortion D , we have

$$\frac{D}{d} = 2 \frac{d^2}{\epsilon^2} \implies \epsilon = d \sqrt{\frac{2d}{D}}.$$

Similarly, for the Gaussian mechanism, we can bound the L_2 sensitivity by \sqrt{d} . For a fixed δ , the privacy risk ϵ for adding Gaussian noise with variance σ^2 is given by

$$\epsilon = 2 \frac{\sqrt{d}}{\sigma} \sqrt{\ln\left(\frac{1.25}{\delta}\right)}.$$

Since we are adding Gaussian noise independently to each pixel, the variance of the per pixel noise is given by $\sigma = \frac{D}{d}$. As a result, we have

$$\epsilon = 2 \frac{d}{\sqrt{D}} \sqrt{\ln\left(\frac{1.25}{\delta}\right)}.$$

F Details of Experiments

We train our models based on the data-driven GAP presented in Section 3 using TensorFlow [Abadi et al., 2016].

F.1 GENKI Dataset

The GENKI dataset consists of 1,740 training and 200 test samples. Each data sample is a 16×16 greyscale face image with varying facial expressions. Both training and test datasets contain 50% male and 50% female. Among each gender, we have 50% smile and 50% non-smile faces. We consider gender as the sensitive variable S and the image pixels as non-sensitive variable X .

ARCHITECTURE. The FNND is modeled by a four-layer feedforward neural network. We first reshape each image to a vector (256×1), and then concatenate it with a 100×1 Gaussian random noise vector. Each entry in the noise vector is sampled independently from a standard Gaussian distribution. We feed the entire vector to a four-layer fully connected (FC) neural network. Each layer has 256 neurons with a leaky ReLU activation function. Finally, we reshape the output of the last layer to a 16×16 image.

To model the TCNND, we first generate a 100×1 Gaussian random vector and use a linear projection to map the noise vector to a $4 \times 4 \times 256$ feature tensor. The feature tensor is then fed to an initial transposed convolution layer (DeCONV) with 128 filters (filter size 3×3 , stride 2) and a ReLU activation, followed by another DeCONV layer with 1 filter (filter size 3×3 , stride 2) and a tanh activation. The output of the DeCONV layer is added to the original image to generate the processed data. For both decorrelators, we add batch normalization [Ioffe and Szegedy, 2015] on each hidden layer to prevent covariance shift and help gradients to flow. We model the adversary using convolutional neural networks (CNNs). This architecture outperforms most of other models for image classification [Krizhevsky et al., 2012, Szegedy et al., 2015].

Figure 18 illustrates the architecture of the adversary. The processed images are fed to two convolution layers (CONV) whose sizes are $3 \times 3 \times 32$ and $3 \times 3 \times 64$, respectively. Each convolution layer is followed by ReLU activation and batch normalization. The output of each convolution layer is fed to a 2×2 maxpool layer (POOL) to extract features for classification. The second maxpool layer is followed by two fully connected layers, each contains 1024 neurons with a batch normalization and a ReLU activation. Finally, the output of the last fully connected layer is mapped to the output layer, which contains two neurons capturing the belief of the subject being a male or a female.

F.2 HAR Dataset

The HAR dataset consists of 561 features of motion sensor data collected by a smartphone from 30 subjects performing six activities (walking, walking upstairs, walking downstairs, sitting, standing, laying). We choose subject identity as sensitive variable S and features of motion sensor data as public variable X . The dataset is randomly partitioned into 8,000 training and 2,299 test samples.

ARCHITECTURE. We first concatenate the original data with a 100×1 Gaussian random noise vector. We then feed the entire 661×1 vector to a Feed Forward neural network with

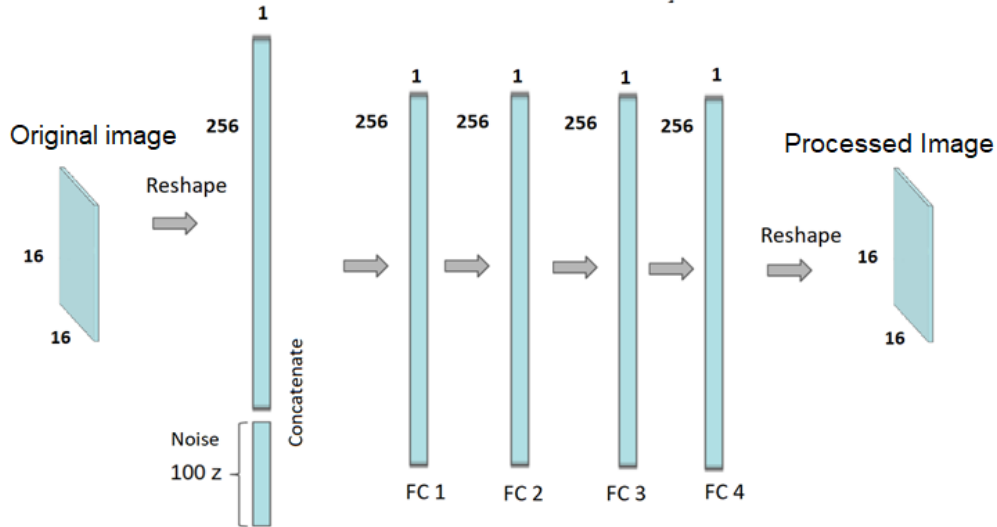


Figure 16: Feedforward neural network decorrelator

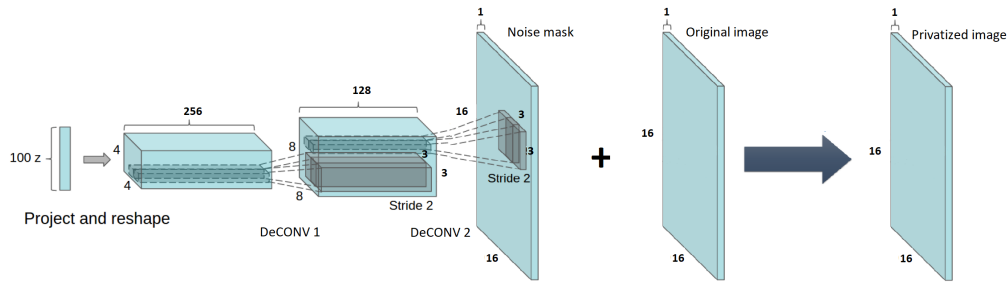


Figure 17: Transposed convolution neural network decorrelator

three hidden fully connected (FC) layers. Each hidden layer has 512 neurons with a leaky ReLU activation. Finally, we use another FC layer with 561 neurons to generate the processed data. For the adversary, we use a five-layer feedforward neural network. The hidden layers have 512, 512, 256, and 128 neurons with leaky ReLU activation, respectively. The output of the last hidden layer is mapped to the output layer, which contains 30 neurons capturing the belief of the subject’s identity. For both decorrelator and adversary, we add a batch normalization after the output of each hidden layer.

F.3 UCI Adult

The UCI Adult dataset consists of 32,561 training and 16,282 testing samples. Each sample has both continuous and categorical features. Table 5 lists all the considered features. We perform an onehot encoding on each categorical feature in (S, X) and store the mapping function from the onehot encoding to the categorical data. For the continuous features in X , we restrict them into the interval $(0, 1)$ by normalization.

ARCHITECTURE. For the UCI Adult dataset, the used architectures are shown in Fig. 19. We concatenate the pre-processed data with a same size standard Gaussian random vector, and feed the entire vector to the encoder. The encoder consists of two full-connected (FC) hidden layers with the number of neurons as 170 and 130, respectively. Since the output representation X_r has the same dimension as the feature variable X , the output layer of the encoder has 113 (as shown

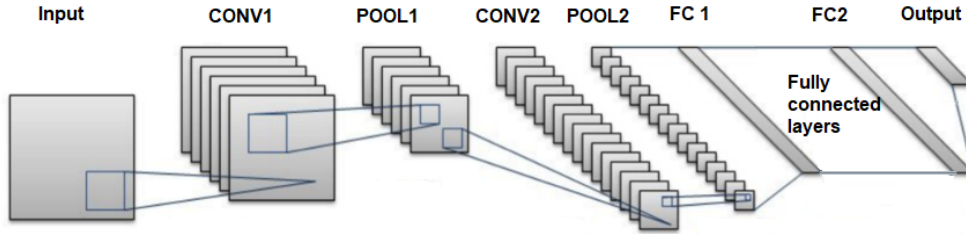


Figure 18: Convolutional neural network adversary

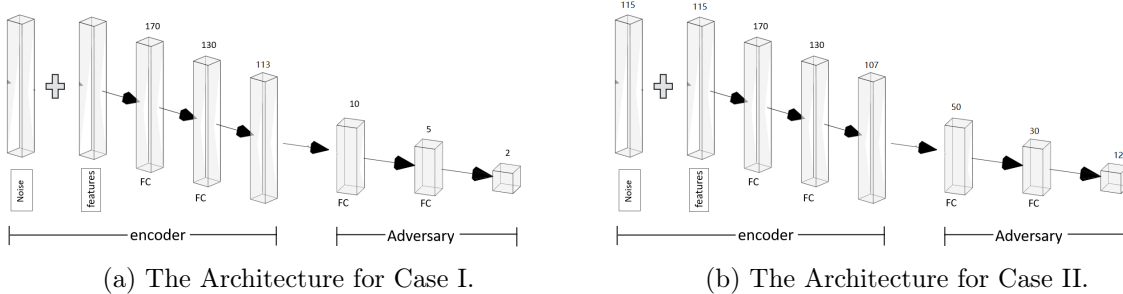


Figure 19: The Architectures of the encoder and adversary for the UCI Adult dataset. Note that the appended noise has the same size of the input features and the output of the encoder has the same dimension as the feature variable X . Therefore, in Fig. 19a, for only taking X into the encoder, the length of the input vector is 226 and for taking both X and the binary S , it is 230. For both scenarios, the length of the encoder’s output is 113. In Fig. 19b, the relationship belongs to the sensitive variable, and therefore, the length of the encoder’s output is 107.

in Fig. 19a) and 107 (as shown in Fig. 19b) neurons for Case I and Case II, respectively. We use a leaky Rectified linear unit (ReLU) activation function in the encoder.

For Case I, the adversarial classifier in Fig. 19a consists of three full-connected (FC) layers with the number of neurons as 10, 5 as well as 2, respectively, and it takes X_r as the input and outputs a belief distribution for the binary sensitive variable S (i.e., gender). Here a ReLU is used as the activation function in the two hidden layers and the soft-max is used in the output layer to generate a belief distribution for gender. The same architecture is used for the downstream application of salary classification. For Case II, the adversarial classifier in Fig. 19b consists of three full-connected (FC) layers with the number of neurons as 50, 30 as well as 12, respectively. Here a Leaky ReLU is used as the activation function in the two hidden layers and the soft-max is used in the output layer. All of the above models use log-loss as the loss function and are optimized by a Adam optimizer.

F.4 UTKFace Dataset

The UTKFace dataset consists of more than 20 thousand 200×200 colorful face images labeled by age, ethnicity and gender. Individuals in the dataset have ages from 0 to 116 year old and are divided into 5 ethnicities: White, Black, Asian, Indian, and Others including Hispanic, Latino and Middle Eastern. We take gender as the sensitive information and take both age and ethnicity as the target information for two downstream applications: age regression and (non-binary) ethnicity classification, respectively. We reshape images as size 64×64 and use 16830 samples with age from 10 to 65 and ethnicity as white, black, Asian or India, 80% of which, i.e., 13464 samples, are used for training.

ARCHITECTURE. For the UTKFace dataset, the used architectures are shown in Figs. 20, 21 and 22. Fig. 20 gives the architecture of GAP which consists of an encoder and an adversarial classifier. The encoder is implemented by a noisy auto-encoder whose encoder transforms the original 64×64 RGB-images to a 4096-dimensional feature vector. Different from standard auto-encoder, which directly feeds the feature vector into the encoder part. Here, the feature vector is mixed with a 4096-dimensional standard normal random vector⁴, and then, fed into a decoder to reconstruct a 64×64 colorful image, which is the GAP representation X_r . Specifically, the encoder part of the autoencoder consists of 4 convolution layers with 128, 64, 64 and 64 output channels, respectively, and 3 2×2 -max pooling layers following the first 3 convolution layers. The encoder part is followed by 2 fully-connected layers with 4096 neurons which mixes the noise and the output feature vector. The following decoder part consists of 5 convolution layers with 64, 64, 64, 128 and 3 output channels, respectively, and 3 2×2 -up-sampling layers following the first 3 convolution layers. The adversarial classifier takes into the GAP representation X_r and outputs the prediction of the sensitive information gender. It consists of 2 convolution layers with 20 and 40 output channels, respectively, 2 2×2 -max pooling layers following each of the convolution layers and 2 full-connected layers with 40 and 2 neurons, respectively. The size of kernels in convolution layers is 3×3 . All convolution and full-connected layers use ReLU as the activation function except the last layers of the decoder and the adversarial which use sigmoid and softmax, respectively. The encoder and adversarial classifier use the square-loss and log-loss as the loss functions, respectively, and both of them are optimized by Adam Optimizer.

Fig. 21 gives the architecture of the downstream non-binary classification for ethnicity. The classifier is built by replacing the top (last) 3 fully-connected layers of the VGG 16 model⁵ pre-trained on ImageNet with two fully-connect layers. The first one layer has 256 neurons with ReLU as the activation function and is followed by a Dropout layer with the rate 0.5, and the second one has 4 neurons with softmax as the activation function. The classifier use log-loss and is optimized by a Stochastic Gradient Descent Optimizer. Fig. 22 shows the architecture for the the downstream application of age regression. The regressor consists of three 3×3 convolution layers with 128, 64 and 32 output channels, three 2×2 -max pooling layers following each of the convolution layers, and three fully-connected layers with 512, 128 and 1 neurons, respectively. All layers use ReLU as the activation function except the last layer which uses a linear activation. The model uses the squared loss as the loss function and is optimized by a Adam Optimizer.

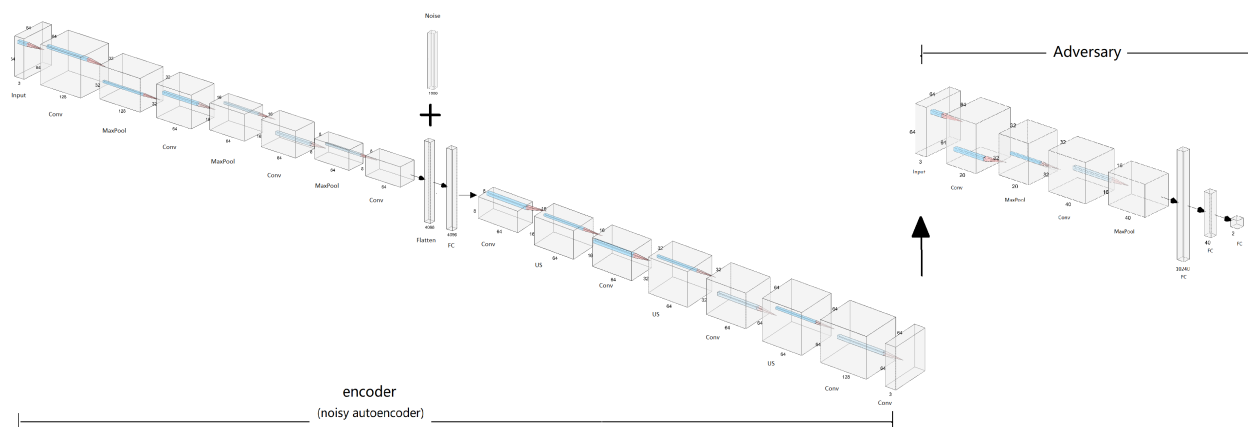


Figure 20: The Architectures of the encoder and adversary for the UTKFace dataset

⁴A random vector is a standard normal random vector if all of its components are independent and identically following the standard normal distribution.

⁵<https://keras.io/applications/#vgg16>

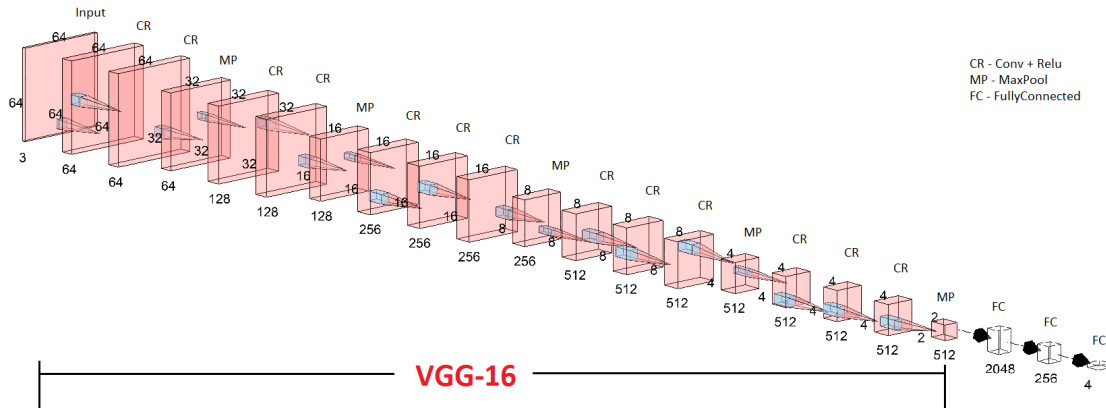


Figure 21: The Architecture of the neural network for ethnicity classification.

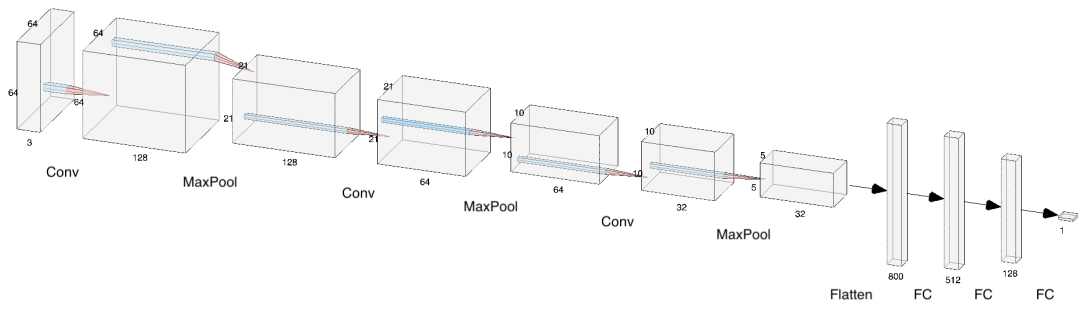


Figure 22: The Architecture of the neural network for age regression.

References

Martín Abadi and David G Andersen. Learning to protect communications with adversarial neural cryptography. *arXiv preprint arXiv:1610.06918*, 2016.

Martín Abadi, Ashish Agarwal, Paul Barham, Eugene Brevdo, Zhifeng Chen, Craig Citro, Greg S Corrado, Andy Davis, Jeffrey Dean, Matthieu Devin, et al. Tensorflow: Large-scale machine learning on heterogeneous distributed systems. *arXiv preprint arXiv:1603.04467*, 2016.

Davide Anguita, Alessandro Ghio, Luca Oneto, Xavier Parra, and Jorge Luis Reyes-Ortiz. A public domain dataset for human activity recognition using smartphones. In *ESANN*, 2013.

Y. O. Basciftci, Y. Wang, and P. Ishwar. On privacy-utility tradeoffs for constrained data release mechanisms. In *2016 Information Theory and Applications Workshop (ITA)*, pages 1–6, Jan 2016. doi: 10.1109/ITA.2016.7888175.

Alex Beutel, Jilin Chen, Zhe Zhao, and Ed H Chi. Data decisions and theoretical implications when adversarially learning fair representations. *arXiv preprint arXiv:1707.00075*, 2017.

F. P. Calmon and N. Fawaz. Privacy against statistical inference. In *Communication, Control, and Computing (Allerton), 2012 50th Annual Allerton Conference on*, pages 1401–1408, 2012.

- Flavio Calmon, Dennis Wei, Bhanukiran Vinzamuri, Karthikeyan Natesan Ramamurthy, and Kush R Varshney. Optimized pre-processing for discrimination prevention. In *Advances in Neural Information Processing Systems*, pages 3992–4001, 2017.
- Xiao Chen, Thomas Navidi, Stefano Ermon, and Ram Rajagopal. Distributed generation of privacy preserving data with user customization. *arXiv:1904.09415*, 2019.
- Elliot Creager, David Madras, Joern-Henrik Jacobsen, Marissa Weis, Kevin Swersky, Toniann Pitassi, and Richard Zemel. Flexibly fair representation learning by disentanglement. In *Proceedings of the 36th International Conference on Machine Learning*, volume 97 of *Proceedings of Machine Learning Research*, pages 1436–1445, Long Beach, California, USA, 09–15 Jun 2019.
- John Duchi, Michael Jordan, and Martin Wainwright. Local privacy and statistical minimax rates. In *Foundations of Computer Science (FOCS), 2013 IEEE 54th Annual Symposium on*, pages 429–438. IEEE, 2013.
- Cynthia Dwork. Differential privacy: A survey of results. In *International Conference on Theory and Applications of Models of Computation*, pages 1–19. Springer, 2008.
- Cynthia Dwork and Aaron Roth. The algorithmic foundations of differential privacy. *Found. Trends Theor. Comput. Sci.*, 9(3–4):211–407, August 2014. ISSN 1551-305X. doi: 10.1561/04000000042. URL <http://dx.doi.org/10.1561/04000000042>.
- Cynthia Dwork, Krishnaram Kenthapadi, Frank McSherry, Ilya Mironov, and Moni Naor. Our data, ourselves: Privacy via distributed noise generation. In *Annual International Conference on the Theory and Applications of Cryptographic Techniques*, pages 486–503. Springer, 2006a.
- Cynthia Dwork, Frank McSherry, Kobbi Nissim, and Adam Smith. Calibrating noise to sensitivity in private data analysis. In *Theory of cryptography conference*, pages 265–284. Springer, 2006b.
- Cynthia Dwork, Moritz Hardt, Toniann Pitassi, Omer Reingold, and Richard Zemel. Fairness through awareness. In *Proceedings of the 3rd innovations in theoretical computer science conference*, pages 214–226. ACM, 2012.
- Jonathan Eckstein and W Yao. Augmented lagrangian and alternating direction methods for convex optimization: A tutorial and some illustrative computational results. *RUTCOR Research Reports*, 32, 2012.
- Harrison Edwards and Amos Storkey. Censoring representations with an adversary. *arXiv preprint arXiv:1511.05897*, 2015.
- Harrison Edwards and Amos Storkey. Censoring representations with an adversary. *arXiv:1511.05897*, 2016.
- Benjamin Fish, Jeremy Kun, and Ádám D Lelkes. A confidence-based approach for balancing fairness and accuracy. In *Proceedings of the 2016 SIAM International Conference on Data Mining*, pages 144–152. SIAM, 2016.
- Robert G Gallager. *Stochastic processes: theory for applications*. Cambridge University Press, 2013.
- AmirEmad Ghassami, Sajad Khodadadian, and Negar Kiyavash. Fairness in supervised learning: An information theoretic approach. *arXiv preprint arXiv:1801.04378*, 2018.

- Ian Goodfellow, Jean Pouget-Abadie, Mehdi Mirza, Bing Xu, David Warde-Farley, Sherjil Ozair, Aaron Courville, and Yoshua Bengio. Generative adversarial nets. In *Advances in neural information processing systems*, pages 2672–2680, 2014.
- Jihun Hamm. Minimax filter: Learning to preserve privacy from inference attacks. *arXiv preprint arXiv:1610.03577*, 2016.
- Moritz Hardt, Eric Price, Nati Srebro, et al. Equality of opportunity in supervised learning. In *Advances in neural information processing systems*, pages 3315–3323, 2016.
- Chong Huang, Peter Kairouz, Xiao Chen, Lalitha Sankar, and Ram Rajagopal. Context-aware generative adversarial privacy. *Entropy*, 19(12):656, 2017.
- Sergey Ioffe and Christian Szegedy. Batch normalization: Accelerating deep network training by reducing internal covariate shift. *arXiv preprint arXiv:1502.03167*, 2015.
- Peter Kairouz, Sewoong Oh, and Pramod Viswanath. Extremal mechanisms for local differential privacy. *J. Mach. Learn. Res.*, 17(1):492–542, January 2016. ISSN 1532-4435. URL <http://dl.acm.org/citation.cfm?id=2946645.2946662>.
- Alexander Kraskov, Harald Stögbauer, and Peter Grassberger. Estimating mutual information. *Physical review E*, 69(6):066138, 2004.
- Alex Krizhevsky, Ilya Sutskever, and Geoffrey E Hinton. Imagenet classification with deep convolutional neural networks. In *Advances in neural information processing systems*, pages 1097–1105, 2012.
- Jiachun Liao, Oliver Kosut, Lalitha Sankar, and Flavio P Calmon. Privacy under hard distortion constraints. *arXiv preprint arXiv:1806.00063*, 2018.
- Walter E Lillo, Mei Heng Loh, Stefen Hui, and Stanislaw H Zak. On solving constrained optimization problems with neural networks: A penalty method approach. *IEEE Transactions on neural networks*, 4(6):931–940, 1993.
- Changchang Liu, Supriyo Chakraborty, and Prateek Mittal. Deepprotect: Enabling inference-based access control on mobile sensing applications. *arXiv preprint arXiv:1702.06159*, 2017.
- David Madras, Elliot Creager, Toniann Pitassi, and Richard Zemel. Learning adversarially fair and transferable representations. *arXiv:1802.06309*, 2018a.
- David Madras, Elliot Creager, Toniann Pitassi, and Richard Zemel. Learning adversarially fair and transferable representations. *arXiv preprint arXiv:1802.06309*, 2018b.
- Mehdi Mirza and Simon Osindero. Conditional generative adversarial nets. *arXiv preprint arXiv:1411.1784*, 2014.
- Tan Nguyen and Scott Sanner. Algorithms for direct 0–1 loss optimization in binary classification. In *International Conference on Machine Learning*, pages 1085–1093, 2013.
- Nisarg Raval, Ashwin Machanavajjhala, and Landon P Cox. Protecting visual secrets using adversarial nets. In *CVPR Workshop Proceedings*, 2017.
- D. Rebollo-Monedero, J. Forne, and J. Domingo-Ferrer. From t-Closeness-Like Privacy to Postrandomization via Information Theory. *IEEE Transactions on Knowledge and Data Engineering*, 22(11):1623–1636, November 2010. ISSN 1041-4347. doi: 10.1109/TKDE.2009.190.

- S. Salamatian, A. Zhang, F. P. Calmon, S. Bhamidipati, N. Fawaz, B. Kveton, P. Oliveira, and N. Taft. Managing your private and public data: Bringing down inference attacks against your privacy. 9(7):1240–1255, 2015. doi: 10.1109/JSTSP.2015.2442227. URL <http://ieeexplore.ieee.org/stamp/stamp.jsp?arnumber=7118663>.
- L. Sankar, S. R. Rajagopalan, and H. V. Poor. Utility-privacy tradeoffs in databases: An information-theoretic approach. *IEEE Transactions on Information Forensics and Security*, 8(6):838–852, 2013. doi: 10.1109/TIFS.2013.2253320.
- Prasanna Sattigeri, Samuel C Hoffman, Vijil Chenthamarakshan, and Kush R Varshney. Fairness gan. *arXiv preprint arXiv:1805.09910*, 2018.
- Christian Szegedy, Wei Liu, Yangqing Jia, Pierre Sermanet, Scott Reed, Dragomir Anguelov, Dumitru Erhan, Vincent Vanhoucke, Andrew Rabinovich, et al. Going deeper with convolutions. *Cvpr*, 2015.
- Ardhendu Tripathy, Ye Wang, and Prakash Ishwar. Privacy-preserving adversarial networks. *arXiv preprint arXiv:1712.07008*, 2017.
- Jacob Whitehill and Javier Movellan. Discriminately decreasing discriminability with learned image filters. In *Computer Vision and Pattern Recognition (CVPR), 2012 IEEE Conference on*, pages 2488–2495. IEEE, 2012.
- Depeng Xu, Shuhan Yuan, Lu Zhang, and Xintao Wu. Fairgan: Fairness-aware generative adversarial networks. *arXiv preprint arXiv:1805.11202*, 2018.
- Rich Zemel, Yu Wu, Kevin Swersky, Toni Pitassi, and Cynthia Dwork. Learning fair representations. In *International Conference on Machine Learning*, pages 325–333, 2013.
- Brian Hu Zhang, Blake Lemoine, and Margaret Mitchell. Mitigating unwanted biases with adversarial learning. *arXiv preprint arXiv:1801.07593*, 2018.

Algorithm 1 Alternating minimax censoring preserving algorithm

Input: dataset \mathcal{D} , distortion parameter D , iteration number T

Output: Optimal generative decorrelator parameter θ_p

procedure ALERNATE MINIMAX(\mathcal{D}, D, T)

Initialize θ_p^1 and θ_a^1

for $t = 1, \dots, T$ **do**

Random minibatch of M datapoints $\{x_{(1)}, \dots, x_{(M)}\}$ drawn from full dataset

Generate $\{\hat{x}_{(1)}, \dots, \hat{x}_{(M)}\}$ via $\hat{x}_{(i)} = g(x_{(i)}, s_{(i)}; \theta_p^t)$

Update the adversary parameter θ_a^{t+1} by stochastic gradient ascend for j epochs

$$\theta_a^{t+1} = \theta_a^t + \alpha_t \nabla_{\theta_a^t} \frac{1}{M} \sum_{i=1}^M -\ell(h(\hat{x}_{(i)}; \theta_a^t), s_{(i)}), \quad \alpha_t > 0$$

Compute the descent direction $\nabla_{\theta_p^t} \ell(\theta_p^t, \theta_a^{t+1})$, where

$$\ell(\theta_p^t, \theta_a^{t+1}) = -\frac{1}{M} \sum_{i=1}^M \ell(h(g(x_{(i)}, s_{(i)}; \theta_p^t); \theta_a^{t+1}), s_{(i)})$$

subject to $\frac{1}{M} \sum_{i=1}^M [d(g(x_{(i)}, s_{(i)}; \theta_p^t), x_{(i)})] \leq D$

Perform line search along $\nabla_{\theta_p^t} \ell(\theta_p^t, \theta_a^{t+1})$ and update

$$\theta_p^{t+1} = \theta_p^t - \alpha_t \nabla_{\theta_p^t} \ell(\theta_p^t, \theta_a^{t+1})$$

Exit if solution converged

return θ_p^{t+1}
